

## Key Points:

- We present an assessment of bulk and component-specific magnetic measurements for sediments deposited under variable redox conditions
- Bulk magnetic parameters provide valuable delineation of continuous environmental variations
- Component-specific techniques enable quantification of individual magnetic mineral assemblages to understand environmental variations

## Supporting Information:

- Supporting Information S1

## Correspondence to:

Y. Qian,  
yao.qian@anu.edu.au

## Citation:

Qian, Y., Roberts, A. P., Liu, Y., Hu, P., Zhao, X., Heslop, D., et al. (2020). Assessment and integration of bulk and component-specific methods for identifying mineral magnetic assemblages in environmental magnetism. *Journal of Geophysical Research: Solid Earth*, 125, e2019JB019024. <https://doi.org/10.1029/2019JB019024>

Received 7 NOV 2019

Accepted 28 JUL 2020

Accepted article online 3 AUG 2020

## Assessment and Integration of Bulk and Component-Specific Methods for Identifying Mineral Magnetic Assemblages in Environmental Magnetism

Yao Qian<sup>1</sup> , Andrew P. Roberts<sup>1</sup> , Yan Liu<sup>2</sup>, Pengxiang Hu<sup>1</sup> , Xiang Zhao<sup>1</sup> , David Heslop<sup>1</sup> , Katharine M. Grant<sup>1</sup>, Eelco J. Rohling<sup>1,3</sup> , Rick Hennekam<sup>4</sup> , and Jinhua Li<sup>2</sup>

<sup>1</sup>Research School of Earth Sciences, Australian National University, Canberra, ACT, Australia, <sup>2</sup>Key Laboratory of Earth and Planetary Physics, Institute of Geology and Geophysics, Chinese Academy of Sciences, Beijing, China, <sup>3</sup>Ocean and Earth Science, University of Southampton, National Oceanography Centre, Southampton, UK, <sup>4</sup>Department of Ocean Systems, NIOZ Royal Netherlands Institute for Sea Research and Utrecht University, Utrecht, The Netherlands

**Abstract** Magnetic parameters are used extensively to interpret magnetic mineral assemblage variations in environmental studies. Conventional room temperature measurements of bulk magnetic parameters, like the anhysteretic remanent magnetization (ARM) and the ratio of the susceptibility of ARM to magnetic susceptibility ( $\chi$ ), can reflect, respectively, magnetic mineral concentration and/or particle size variations in sediments, although they are not necessarily well suited for identifying magnetic components within individual magnetic mineral assemblages. More advanced techniques, such as first-order reversal curve (FORC) diagrams and low-temperature (LT) magnetic measurements, can enable detailed discrimination of magnetic assemblages. Here, we integrate conventional bulk magnetic measurements alongside FORC diagrams, LT measurements, and X-ray fluorescence core-scan data, transmission electron microscope observations, and principal component analysis of FORC diagrams to identify and quantify magnetic mineral assemblages in eastern Mediterranean sediments. The studied sediments were selected because they contain complexly varying mixtures of detrital, biogenic, and diagenetically altered magnetic mineral assemblages that were deposited under varying oxic (organic-poor marls) to anoxic (organic-rich sapropels) conditions. Conventional bulk magnetic parameters provide continuous records of environmental magnetic variations, while more time-consuming LT and FORC measurements on selected samples provide direct ground-truthing of mineral magnetic assemblages that enables calculation of magnetization contributions of different end members. Thus, a combination of conventional bulk parameters and advanced magnetic techniques can provide detailed records from which the meaning of environmental magnetic signals can be unlocked.

### 1. Introduction

Magnetic parameters have been used widely in paleoenvironmental studies since the 1980s (e.g., Kent, 1982; Thompson et al., 1980) to detect variations in minute quantities of magnetic minerals within sedimentary strata. For example, Banerjee et al. (1981) proposed that the ratio of the susceptibility of anhysteretic remanent magnetization ( $\chi_{ARM}$ ) to magnetic susceptibility ( $\chi$ ) can be used for rapid estimation of magnetic grain size variations. Parameters such as  $\chi$ ,  $\chi_{ARM}$ , and the isothermal remanent magnetization (IRM) or saturation IRM (SIRM) are used commonly to indicate variations in the concentration of magnetic particles (e.g., Evans & Heller, 2003; Q. Liu, Roberts, et al., 2012; Maher & Thompson, 1999; Thompson & Oldfield, 1986; Verosub & Roberts, 1995). These parameters are generally measured at room temperature with focus on detecting ferrimagnetic minerals. More advanced methods such as first-order-reversal curve (FORC) (Pike et al., 1999; Roberts et al., 2000) and low-temperature (LT) magnetic measurements (e.g., Chang et al., 2016; Passier & Dekkers, 2002) are more time-consuming but can provide more detailed information for characterizing magnetic mineral assemblages. Supplementary transmission electron microscope (TEM) observations are also valuable for confirming the mineralogy of identified magnetic assemblages. FORC diagrams provide empirical information about the distributions of coercivities ( $B_c$ ) and local interaction fields ( $B_u$ ) for magnetic particle assemblages. For example, Yamazaki (2008) semiquantitatively estimated the relative abundances of a noninteracting single-domain (SD) component and an interacting SD component in North Pacific Ocean sediments using FORC diagrams and

concluded that  $\chi_{\text{ARM}}/\text{SIRM}$  does not necessarily reflect magnetic particle size due to the dependence of ARM acquisition on magnetostatic interactions.

Although advanced magnetic techniques, such as LT and FORC measurements, can provide more information on magnetic mineral assemblages within natural samples compared to conventional bulk magnetic parameters, their interpretations are often based on qualitative assessments and empirical “fingerprinting” (Harrison et al., 2018; Heslop, 2015). Recently, application of principal component analysis (PCA) to analyze FORC diagrams for large sample sets (FORC-PCA), as introduced by Lascu et al. (2015), has been used to discriminate magnetic mineral assemblages in sediments. For example, Channell et al. (2016) applied FORC-PCA to unmix biogenic and detrital magnetic assemblages of a sediment core from Rockall Trough to characterize glacial/interglacial sedimentation on the Northwest Iberian margin. Harrison et al. (2018) further improved the FORC-PCA method to capture both reversible and irreversible magnetization contributions and provided objective criteria to aid identification of physically realistic end members. Roberts et al. (2018) also used FORC-PCA to illustrate how magnetic properties can be used to assess diagenetic processes in reducing sedimentary environments.

In the eastern Mediterranean Sea, organic-rich sedimentary intervals known as sapropels are intercalated cyclically with marls (organic-poor sediments) from the Late Miocene to the Holocene (Emeis et al., 1996, 2000; Hilgen, 1991; Larrasoana, Roberts, Rohling, et al., 2003; Q. S. Liu, Larrasoana, et al., 2012; Lourens et al., 1996; Rohling, 1994; Rohling et al., 2015; Schenau et al., 1999). Sapropels formed during phases of enhanced surface ocean productivity caused by large fluvial discharge events during North African monsoon maxima (Rossignol-Strick, 1983, 1985; Rossignol-Strick et al., 1982). Increased sedimentary organic matter preservation and its subsequent microbial degradation leads to complex postdepositional diagenesis (Larrasoana et al., 2006; Larrasoana, Roberts, Rohling, et al., 2003; Q. S. Liu, Larrasoana, et al., 2012; Passier et al., 2001; Roberts et al., 1999; van Santvoort et al., 1997). Sapropels were deposited under anoxic sulfidic conditions, which promotes reductive dissolution of magnetic minerals (Dekkers et al., 1994; van Santvoort et al., 1997). When sulfate-reducing conditions are strong, excess sulfide diffuses downward into underlying marls, forming a “dissolution front” (Larrasoana et al., 2006; Passier et al., 2001). Mediterranean bottom waters were reoxygenated at the end of periods of sapropel formation and an “oxidation front” then formed at the top of the most recent organic-rich layer (de Lange et al., 2008; Higgs et al., 1994; Larrasoana et al., 2006; Larrasoana, Roberts, Rohling, et al., 2003; Q. S. Liu, Larrasoana, et al., 2012; Passier et al., 2001; Thomson et al., 1999). Subsequently,  $\text{Fe}^{2+}$  in sapropels is oxidized to form iron oxides, which can enhance the magnetization at oxidation fronts above sapropels (Larrasoana et al., 2006; Larrasoana, Roberts, Rohling, et al., 2003; Q. S. Liu, Larrasoana, et al., 2012; Passier & Dekkers, 2002). Between sapropels, marls supplied by eolian dust and fluvial inputs are deposited under oxic conditions. Therefore, eastern Mediterranean sediments contain complex mixtures of detrital and diagenetically altered magnetic minerals, and potentially biogenic magnetite, that make them a suitable subject for evaluating the effectiveness of a series of advanced techniques used in environmental magnetism compared to conventional bulk magnetic parameters.

Magnetic mineral variations have been identified in sapropel-bearing eastern Mediterranean sediments through bulk magnetic measurements and diffuse reflectance spectroscopy (Heslop et al., 2007; Kruiver & Passier, 2001; Larrasoana et al., 2006; Larrasoana, Roberts, Rohling, et al., 2003; Q. S. Liu, Larrasoana, et al., 2012; Passier et al., 2001; Roberts et al., 1999). However, ambiguity remains concerning some important environmental magnetic processes. For example, it has been suggested that enhanced concentrations of biogenic magnetite produced by magnetotactic bacteria (MTB) occur at oxidation fronts above sapropels (Kruiver & Passier, 2001; Passier et al., 2001), but this interpretation has not been confirmed directly by TEM observations. Magnetic mineral dissolution has been reported in sapropels and within dissolution intervals below sapropels (Channell & Hawthorne, 1990; Larrasoana et al., 2006; Larrasoana, Roberts, Rohling, et al., 2003; Passier et al., 2001; Roberts et al., 1999), where the extent to which magnetic minerals were dissolved depends on the intensity of sulfidization. These issues can be addressed by detailed analyses of magnetic mineral assemblages in eastern Mediterranean sediments with advanced environmental magnetic techniques as presented here. In this study, we integrate high-resolution bulk magnetic, FORC, and LT magnetic measurements, TEM observations, and FORC-PCA in conjunction with published calibrated X-ray fluorescence (XRF) core-scan data (Grant et al., 2017) to investigate magnetic mineral assemblages

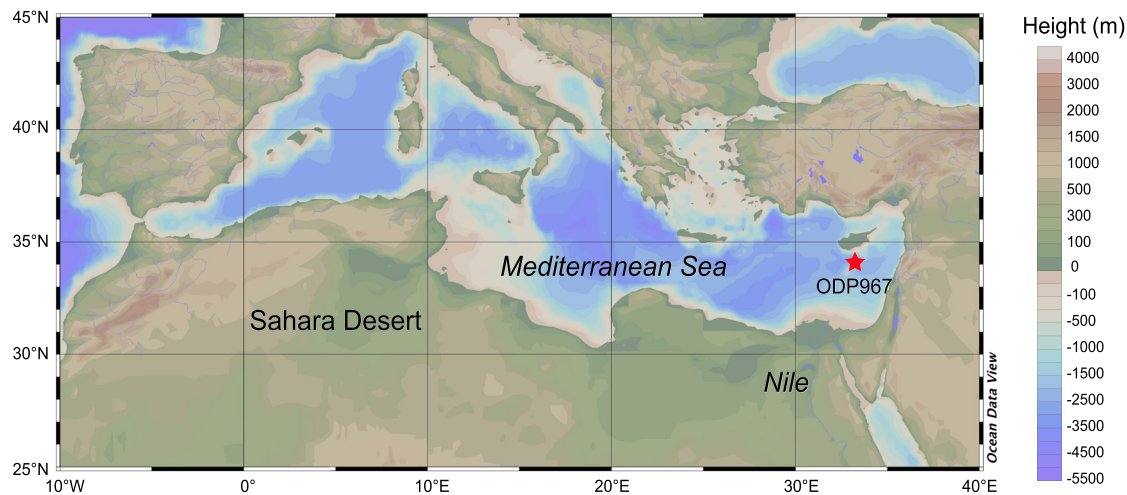


**Figure 1.** Location of ODP Site 967 from which sediments were collected and analyzed in this study. The map was generated with Ocean Data View (Schlitzer, 2014).

within sapropel-bearing sediments from the eastern Mediterranean Sea. Our aim is to make use of the variable magnetic mineral content of eastern Mediterranean sediments to assess the information provided by bulk and component-specific methods to cross-compare and illustrate the benefits of both approaches in identifying mineral magnetic assemblages in environmental magnetism.

## 2. Samples and Methods

### 2.1. Samples

The studied eastern Mediterranean sediments contain complex magnetic mineral mixtures with detrital and diagenetically altered phases, and potentially biogenic magnetite, which are encountered widely in different geologic settings. These sediments were collected from Ocean Drilling Program (ODP) Site 967 (34°04'N, 32°43'E, water depth 2,553 m), which was recovered during ODP Leg 160 (Shipboard Scientific Party, 1996) on the northern slope of Eratosthenes Seamount (Figure 1). Core sections were sampled with “u-channels” from the archive halves of cores along a continuous composite section (Sakamoto et al., 1998) at the IODP core repository in Bremen, Germany, in 1995 and have been kept in cold storage since sampling. U-channel measurements used here are from Stoner et al. (1998) and were made within 2 years of sampling. To obtain higher-resolution measurements in this study, u-channel samples were sliced at 1-cm intervals into discrete nonmagnetic 2 × 2 × 2 cm plastic cubes and were stored thereafter in a refrigerator. The studied sequence, from Hole 967C core sections 5H6 to 5H7, spans approximately 2.7 m, which occurs at depths of between 49.99 and 52.69 m based on the composite depth section of Grant et al. (2017). This interval ranges in age from 1.59 to 1.71 Ma based on the age model of Grant et al. (2017) for Site 967. Five sapropels of two types occur in this interval (Figure 2). These two types of sapropels are representative sapropels (“Type 2” sapropels with both oxidation and dissolution intervals in the classification of Larrasoana, Roberts, Stoner, et al. (2003); dark gray shaded bars in Figures 2–7) and weakly developed sapropels (“Type 3” sapropels without dissolution intervals in the classification of Larrasoana, Roberts, Stoner, et al. (2003); light gray shaded bars in Figures 2–7). A total of 221 discrete samples were collected for bulk environmental magnetic measurements across the studied stratigraphic interval. Based on bulk magnetic results, 34 samples were selected for more detailed analyses and were packed into nonmagnetic gelatin-capsules for FORC measurements (green circles, Figure 3). A further five samples were chosen for LT and TEM analyses (black circles, Figure 3) (see Table S1 in the supporting information).

### 2.2. Storage Diagenesis

Changes in sediment magnetic properties can occur when organic-rich sediments oxidize during storage (e.g., Oldfield et al., 1992; Richter et al., 1999). Such susceptibility or remanence losses are referred to as “storage diagenesis” (Oldfield et al., 1992). Roberts et al. (1999) observed marked susceptibility and remanence losses in Pliocene eastern Mediterranean sapropels, which Reinholdsson et al. (2013) suggested could have

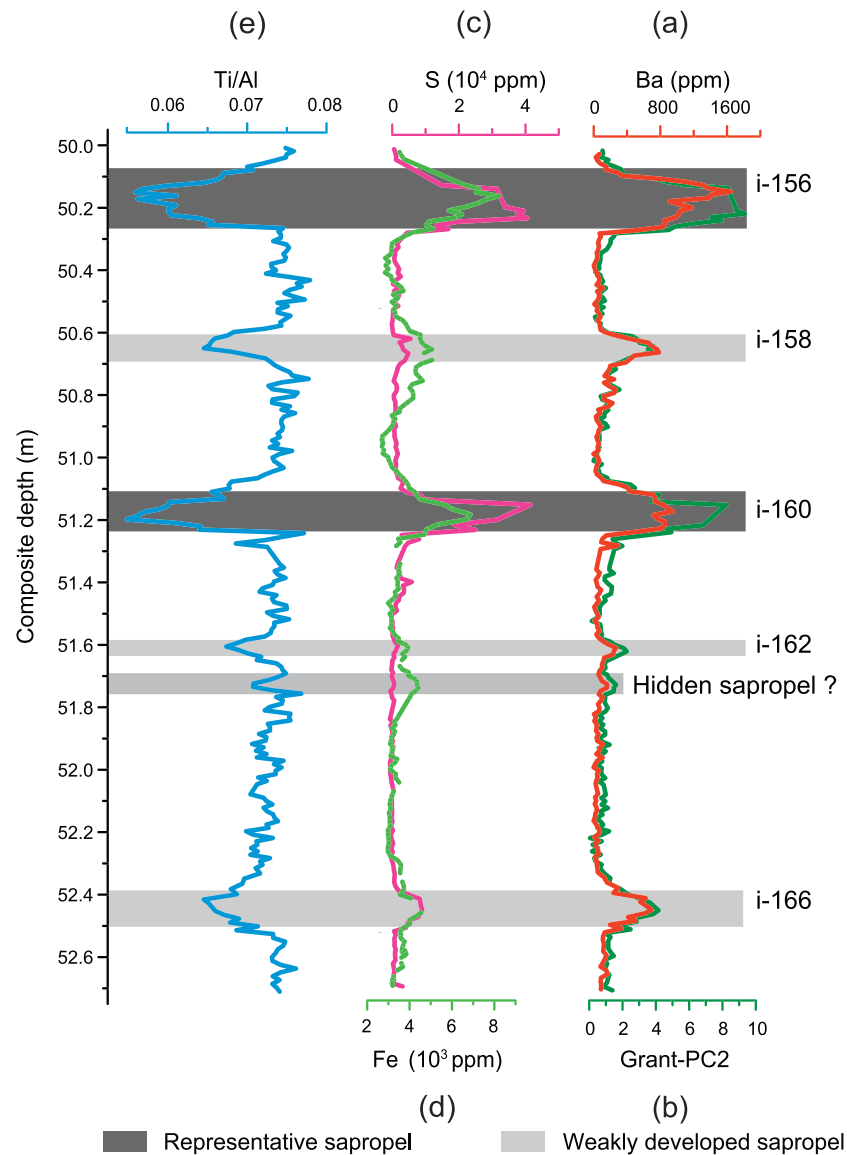


**Figure 2.** Geochemical data from ODP Site 967 for sediments between 1.59 and 1.71 Ma (Grant et al., 2017). (a, b) Elevated Ba (orange) and Grant-PC2 (dark green) indicate sapropel boundaries (see Thomson et al., 1995, and Nijenhuis et al., 1999), where Grant-PC2 represents the use of PCA by Grant et al. (2017) to detect sapropel boundaries based on a combination of several elements; (c) S concentration (pink); (d) Fe concentration (light green); (e) Ti/Al ratio (blue). Dark gray shaded bars indicate the positions of representative sapropels. Light gray shaded bars indicate the positions of weakly developed sapropels. A bar with intermediate gray shading indicates the position of a suspected “hidden” sapropel with minor Ba enrichment. Sapropel stratigraphy is after Emeis et al. (2000), where “i-” followed by a number denotes the insolation cycle represented by the identified sapropels.

been caused by the oxidation of biogenic greigite during storage. Observation of these losses in eastern Mediterranean sapropel-bearing sequences makes it reasonable to check whether other sediments recovered during ODP Leg 160 experienced similar losses. Marked remanence losses are evident when shipboard measurements are compared with U-channel measurements made within 2 years of sampling for Sites 966, 967, and 969 (Stoner et al., 1998). Remanence losses are most marked for Site 966; we calculate here that on average only 1% of the shipboard natural remanent magnetization (NRM) remained in the measurements of Stoner et al. (1998) for Site 966.

To assess remanence losses for the studied interval of Site 967, we compare shipboard whole-core magnetic susceptibility measurements that were made before the cores were split (Emeis et al., 1996) with our discrete

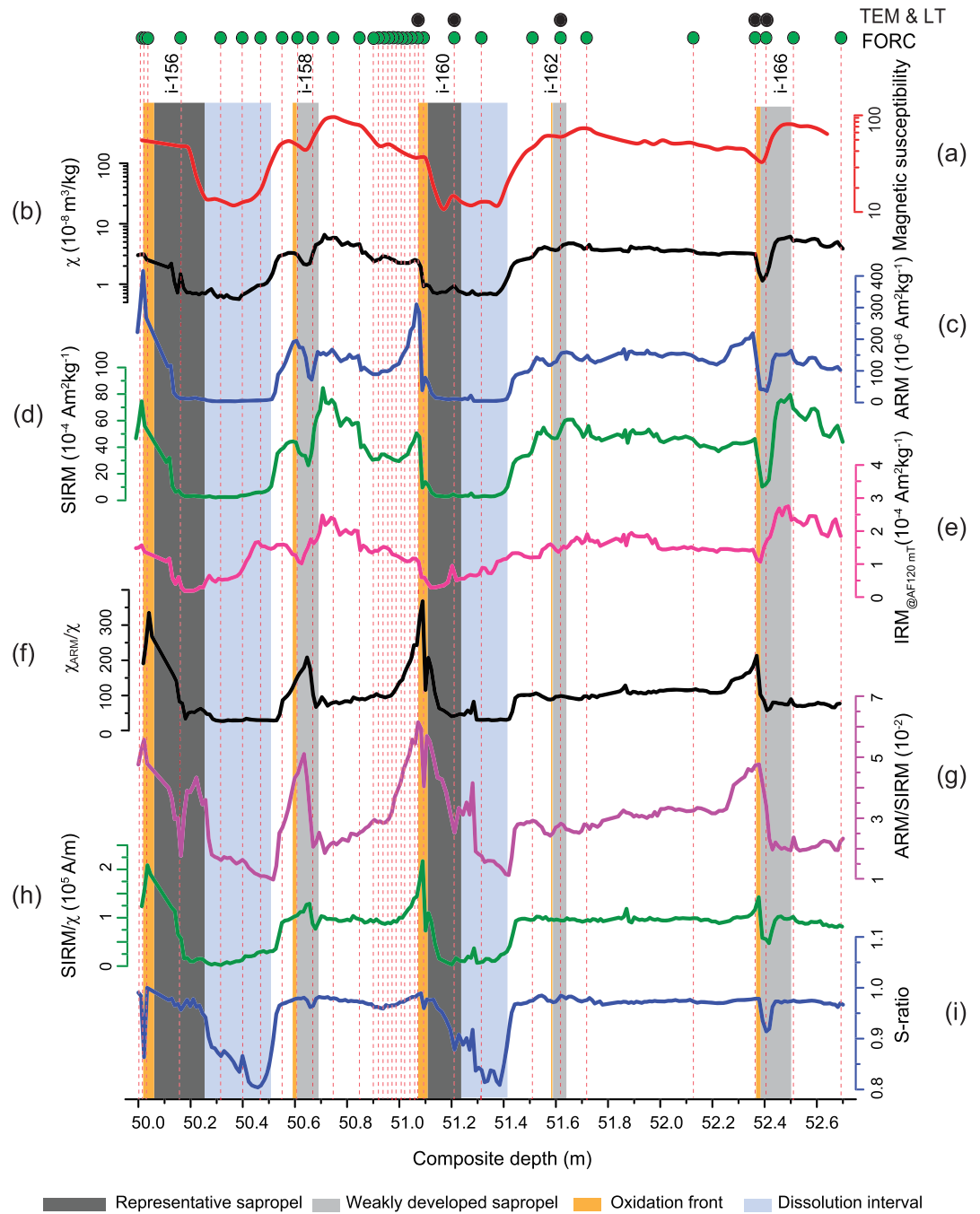


**Figure 3.** Down-core variations of magnetic mineral concentration, particle size, and coercivity parameters. For methods used for magnetic measurements, see section 2.2. (a) Shipboard whole-core magnetic susceptibility data for C5H6 and C5H7 from Emeis et al. (1996) (uncorrected instrument units; red); discrete sample data, including (b)  $\chi$  (black), (c) ARM (blue), (d) SIRM (green), (e)  $IRM_{@AF120\text{ mT}}$  (magenta), (f)  $\chi_{ARM}/\chi$  (black), (g) ARM/SIRM (purple), (h) SIRM/ $\chi$  (green), and (i) S-ratio (dark blue). Thirty-four green circles (top) indicate the locations of samples subjected to FORC measurements and five black circles (top) represent the locations of samples subjected to LT measurements and TEM observations. As indicated in Figure 2, dark gray shaded bars indicate the positions of representative sapropels, light gray shaded bars indicate the positions of weakly developed sapropels, orange shading above sapropels indicates the positions of oxidation fronts, and light blue shading below representative sapropels indicates the positions of dissolution intervals. Sapropel stratigraphy is after Emeis et al. (2000).

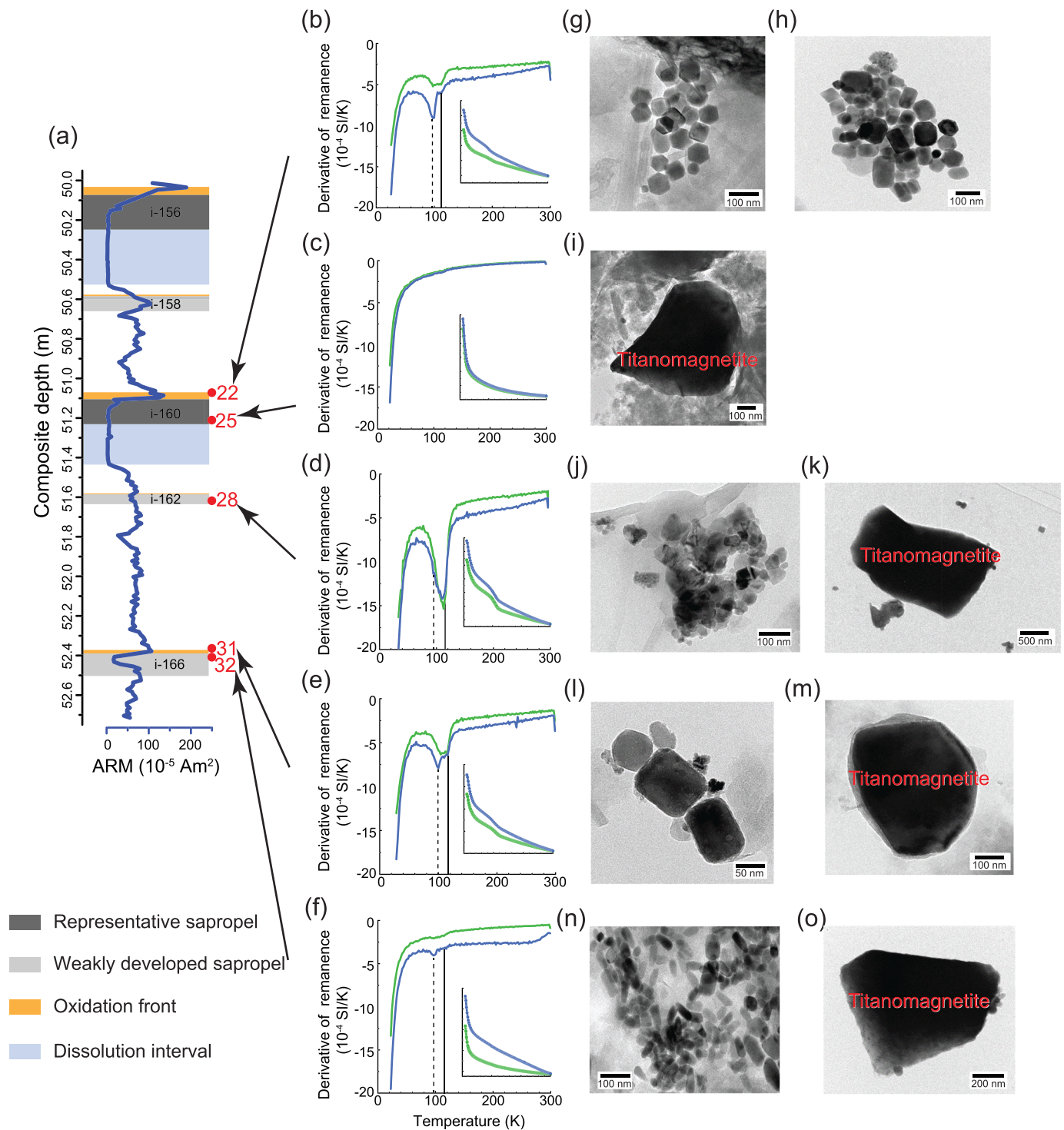


**Figure 4.** LT magnetic measurements and TEM observations for five representative samples. (a) The locations of the five samples are indicated on an ARM profile with sapropel stratigraphy after Emeis et al. (2000). (b–f) LT magnetization curves (inset) and their derivative curves (larger; ZFC, green; FC, blue). Vertical dashed and solid lines indicate the two distinctive  $T_V$  peaks at  $\sim 95$  and  $\sim 110$  K, respectively. (g, h) TEM images for Sample 22 from the oxidation front of representative sapropel i-160 with abundant magnetosomal magnetite; (i) TEM image for Sample 25 from the middle of sapropel i-160 with a detrital titanomagnetite particle; (j, k) TEM images for Sample 28 from the middle of weakly developed sapropel i-162 with both magnetosomal magnetite and titanomagnetite; (l, m) TEM images for Sample 31 from the oxidation front above weakly developed sapropel i-166 with clusters of biogenic magnetite and detrital titanomagnetite; and (n, o) TEM images for Sample 32 from the middle of weakly developed sapropel i-166 with abundant bullet-shaped biogenic magnetite and detrital titanomagnetite. TEM electron dispersive X-ray (TEM-EDX) spectra are indicative of mineralogy, as shown in Figure S2.

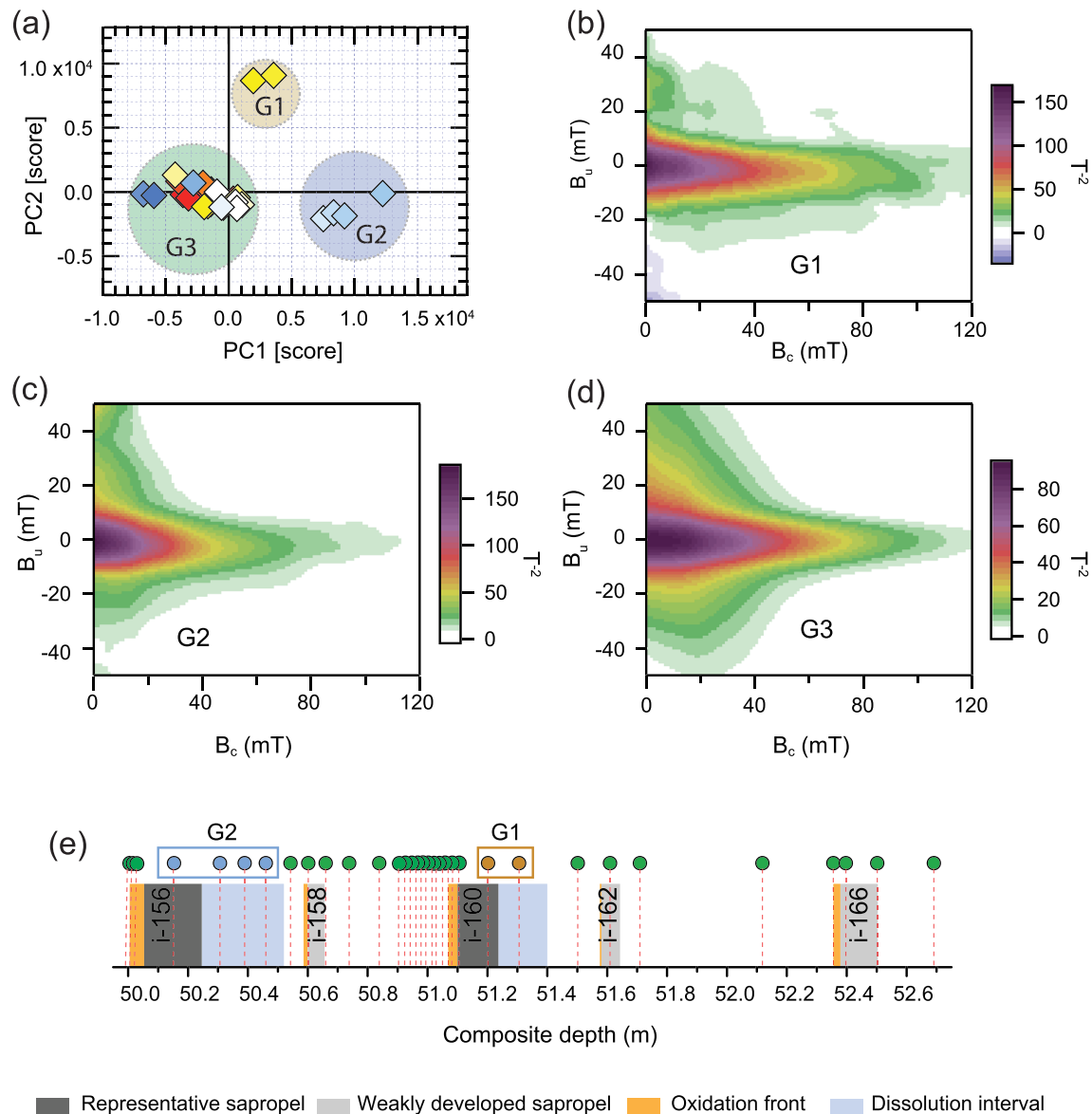


**Figure 5.** FORC-PCA results for 34 selected samples. (a) Distribution of sample PC scores in PC1-PC2 space, from which three groups (G1, G2, and G3) are defined. Diamonds represent the PC scores for the measured FORC data, which are shown with respect to the two principal components (PC1 and PC2); (b) FORC distribution for a typical G1 sample, which has dominantly stable SD behavior; (c) FORC distribution for a typical G2 sample, which contains mixed stable SD and vortex state behavior; (d) FORC distribution for a typical G3 sample, which also contains mixed stable SD and vortex state components due to biogenic and detrital magnetite, respectively; and (e) stratigraphic locations of samples from each group: G1 (orange), G2 (light blue), and G3 (green) in the studied sequence. Dark gray shaded bars indicate the positions of representative sapropels. Light gray shaded bars indicate the positions of weakly developed sapropels. Light blue shading below the sapropels marks the positions of dissolution intervals, while orange shading above the sapropels indicates the positions of oxidation fronts. Sapropel stratigraphy is after Emeis et al. (2000).

sample measurements made >20 years later (Figures 3a and 3b). Cross-calibration of volume- and mass-normalized susceptibility results has not been undertaken, but similar variations between the two data sets indicate that any storage diagenesis in the studied intervals has not obscured expression of the magnetic property cycles studied here. Comparison of shipboard NRM measurements after AF demagnetization at 25 mT (the only shipboard remanence measurement made) with the U-channel measurements of Stoner et al. (1998) for the interval of Site 967 studied here indicates that on average only 41% of the initial NRM remained at the time of u-channel measurement (for 28 measurement points) (Figure S1a). The original NRM cyclicity associated with variations through sapropels is clearly evident in

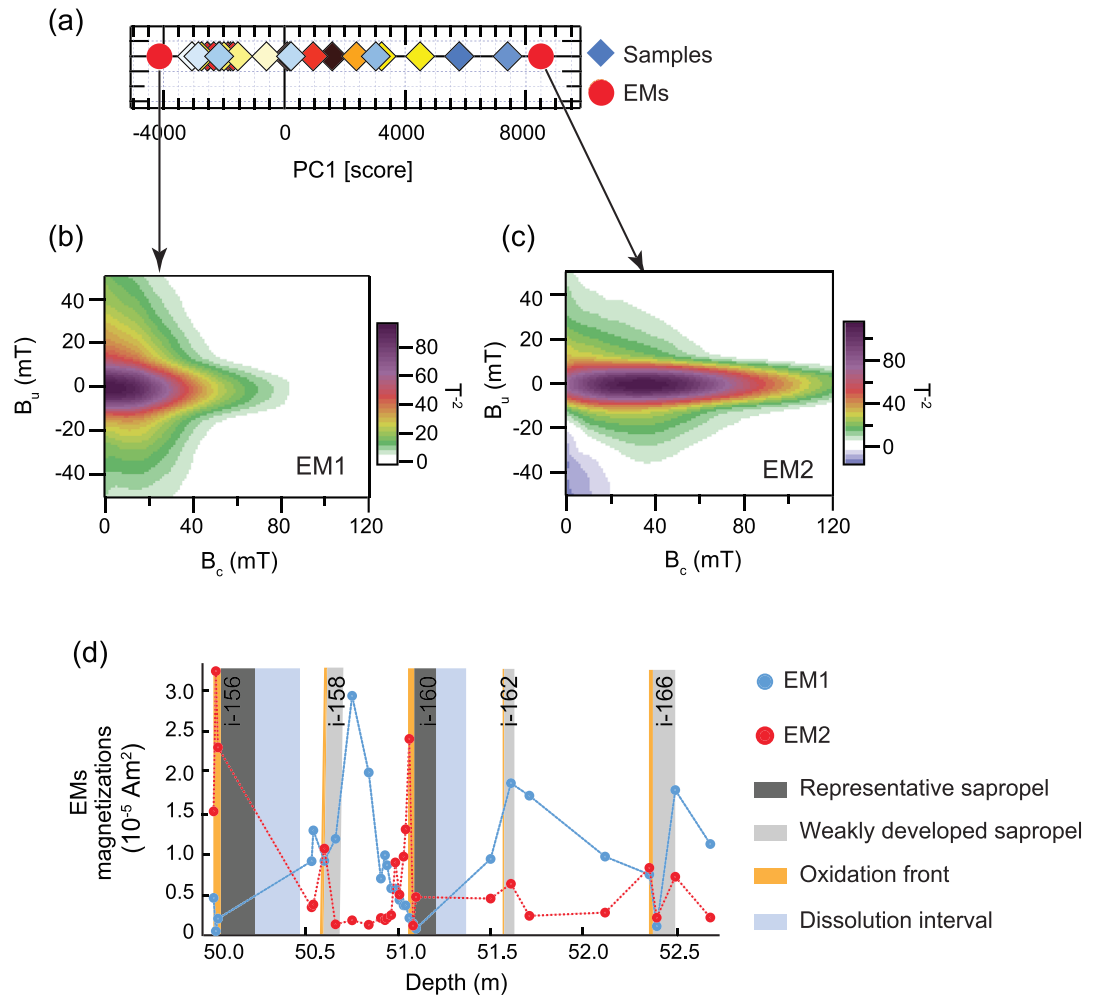


**Figure 6.** FORC-PCA results for samples from Group 3 (G3) samples in Figure 5, which is treated as a linear combination of two EMs. (a) Distribution of PC scores for 28 samples in PC1 space with FORC diagrams for the two EMs (the color coding for diamond symbols is the same as in Figure 5a); (b) EM1 consists of dominantly vortex state particles; (c) EM2 consists of dominantly noninteracting SD behavior; and (d) magnetizations of EM1 (blue) and EM2 (red) calculated from FORC-PCA unmixing and presented with respect to depth.

both data sets in Figure S1a. We did not measure the NRM in this study, so we compare our ARM data for Hole 967C with those from Stoner et al. (1998), which were measured on equivalent sections of Hole 967B (Figure S1b). Despite the fact that the measurements are not from identical sediments, there is good agreement between the data sets with no evidence for further remanence loss. The amplitude of ARM variations for the discrete samples is larger, as would be expected because they are less smoothed. These data confirm that storage diagenesis appears to have been associated with early drying of the cores and that minimal remanence loss has occurred in the intervening 20+ years.

Oldfield et al. (1992) demonstrated that remanence losses will occur in association with iron oxide oxidation during dehydration of organic-rich sediments and that such losses are not necessarily an indicator of greigite oxidation. The fact that remanence losses are observed throughout the studied sediment interval (Figure S1a), including within sapropels and intervening oxic sediments, is consistent with the interpretation of Oldfield et al. (1992). We, therefore, interpret the observed storage diagenesis as indicating losses to most of the magnetic mineral fraction. Despite these losses, original cyclicities are preserved and our results below reveal the presence of original detrital and biogenic magnetic minerals, with magnetic variations driven by nonsteady-state diagenesis. We analyzed the studied sediments for the case study presented here because they contain these variations, which are evident regardless of the effects of storage diagenesis.

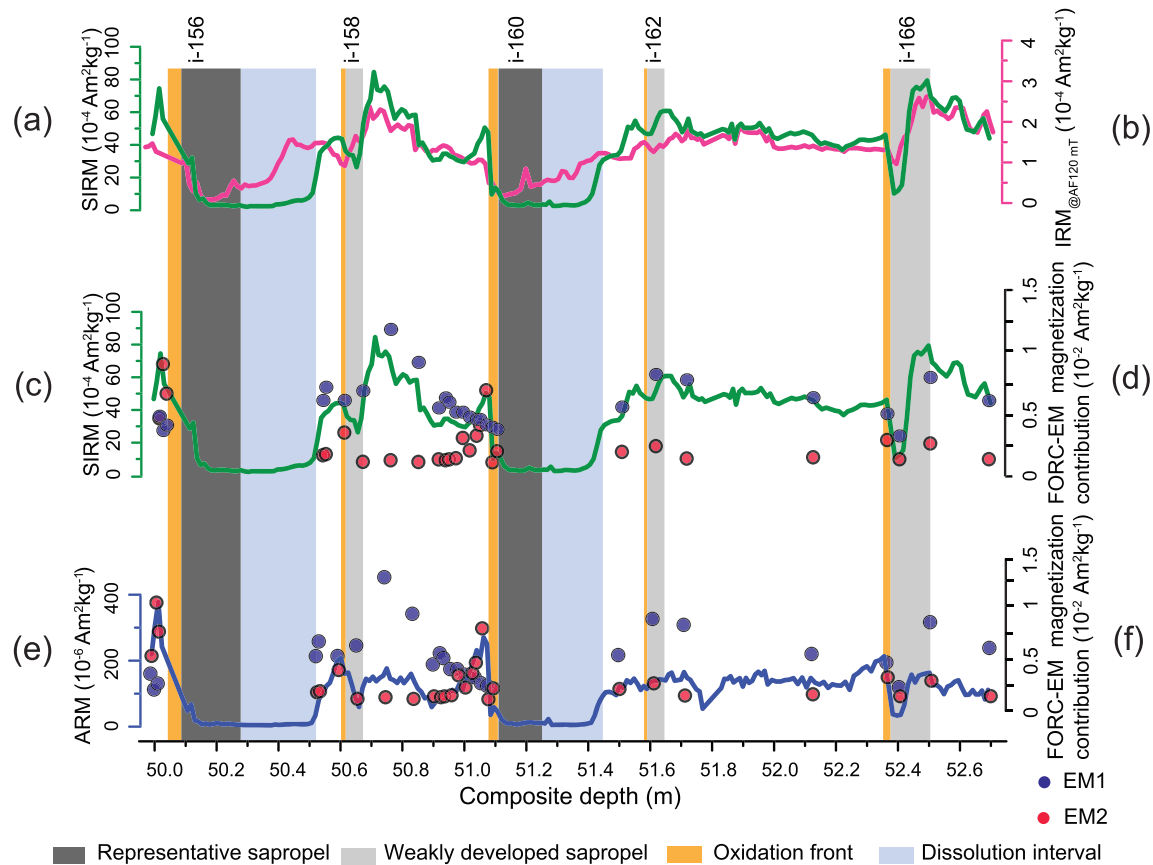


**Figure 7.** (a, c) SIRM (green) and (b)  $IRM_{@AF120\text{ mT}}$  (magenta), which is used as a proxy for Saharan dust in the eastern Mediterranean Sea (Larrasoña, Roberts, Rohling, et al., 2003); (d, f) FORC-EM magnetization contribution, which is overlain on (c) SIRM and (e) ARM curves to illustrate their similar trends, where ARM represents the ferrimagnetic mineral concentration (blue). Blue and red circles represent EM1 (vortex state detrital magnetite) and EM2 (biogenic magnetite), respectively, as defined in Figure 6. Dark gray shaded bars indicate the positions of representative sapropels. Light gray shaded bars indicate the positions of weakly developed sapropels. Light blue shading below sapropels marks the positions of dissolution fronts; orange shading above sapropels indicates the positions of oxidation fronts. Sapropel stratigraphy is after Emeis et al. (2000).

Magnetic enhancement has been reported in Type 1 sapropels (Roberts et al., 1999) in the classification of Larrasoña, Roberts, Stoner, et al. (2003), which has been attributed by Reinholdsson et al. (2013) as due to the presence of biogenic greigite. We avoided Type 1 sapropels in this study because they are dominated by major remanence losses and do not have the variable magnetic properties observed in Types 2 and 3 sapropels on which we focus here.

### 2.3. Magnetic Measurements

Magnetic measurements were made at the Paleomagnetism Laboratory, Australian National University (ANU). Magnetic susceptibility was measured using a Kappabridge KLY-3 magnetic susceptibility meter (875 Hz) and the mass-specific  $\chi$  was calculated. An ARM was imparted to samples with a direct current (DC) bias field of 0.05 mT and a peak alternating field (AF) of 100 mT.  $\chi_{ARM}$  was calculated by normalizing ARM to the DC-bias field.  $IRM_{900\text{ mT}}$  was imparted with an induction field of 900 mT to represent SIRM, and  $IRM_{-0.3\text{ T}}$  was imparted with a backfield of 0.3 T.  $IRM_{@AF120\text{ mT}}$  was obtained after AF demagnetization of the SIRM at 120 mT, which represents the high-coercivity hematite contribution (Larrasoña, Roberts, Rohling, et al., 2003). The interparametric ratios  $\chi_{ARM}/\chi$ ,  $ARM/SIRM$ , and  $SIRM/\chi$  were calculated to represent magnetic grain size variations (J. King et al., 1982; J. W. King & Channell, 1991). The S-ratio is calculated as  $0.5 \times [1 - (IRM_{-0.3T}/SIRM)]$ , which provides a measure of the relative abundance of low- to high-coercivity minerals (Bloemendal et al., 1992).

FORC measurements were made with a Princeton Measurements Corporation MicroMag vibrating sample magnetometer (VSM; Model 3900) using the irregular grid FORC protocol (Zhao et al., 2015). An averaging time of 300 ms was used for samples with remanent magnetizations less than  $1 \mu\text{Am}^2$  and a 200 ms averaging time was used for more strongly magnetized samples. FORC diagrams were processed using the xFORC software (Zhao et al., 2015). A smoothing factor (SF) of 3 or 4 was used depending on the noise level of samples. FORC data were imported into the FORCinel algorithm (Harrison & Feinberg, 2008) for FORC-PCA analysis (Harrison et al., 2018) and VARIFORC smoothing (Egli, 2013) was used for processing ( $S_{c0} = 3$ ,  $S_{c1} = 3$ ,  $S_{b0} = 4$ ,  $S_{b1} = 4$ ,  $\lambda_b = 0.1$ ,  $\lambda_c = 0.1$ ). FORCs were resampled from the irregular measurement grid to a 0.25-mT regular grid for PCA. End Members (EMs) were selected by defining a mixing space that bounds all data, with parsimonious selection of vertices that do not fall far from the data, and with guidance from the feasibility metrics of Harrison et al. (2018) that constrain solutions to fall within a physically realistic space (with monotonic changes of FORCs and without crossing of curves). EM mixing proportions and absolute contributions to the saturation magnetization were calculated based on the solution.

LT magnetic measurements were made with a Quantum Design Magnetic Property Measurement System (MPMS; model XL7). Zero-field-cooled (ZFC) and field-cooled (FC) magnetizations were measured during warming from 5 to 300 K at 1-K intervals. Samples were first cooled to 5 K in a zero-field environment. A 5-T DC field was then applied and was switched off to impart an SIRM. SIRM curves were measured to 300 K at a heating rate of 1 K/min. A FC magnetization curve was then measured by applying a 5-T DC field throughout cooling from room temperature to 5 K. At 5 K, the field was switched off and the SIRM was then measured back to 300 K at a heating rate of 1 K/min.

#### 2.4. TEM Observations

Magnetic mineral extracts were obtained from bulk sediments by stirring the powdered sediment within a small volume of distilled water before thoroughly dispersing the slurry by ultrasonication. Magnetic particles were then extracted with a magnetic finger (rare Earth magnet). To concentrate and purify magnetic particles, the extraction procedure was repeated at least five times. Magnetic extracts were viewed and analyzed using a JEM-2100HR TEM operating at 200 kV, with the electron beam generated from a LaB<sub>6</sub> gun at the Institute of Geology and Geophysics, Chinese Academy of Sciences.

### 3. XRF-Core-Scanning and Sapropel Identification

We use the XRF core-scanning data of Grant et al. (2016, 2017) to identify sapropels, which are delineated clearly based on Ba variations (Grant et al., 2016) and Grant-PC2, which is principal component 2 from sediment geochemical data, as used by Grant et al. (2017) (Figures 2a and 2b). Grant-PC2 corresponds to elements associated with sapropels and their various redox states and provides a more comprehensive indication of sediment geochemical changes associated with sapropel deposition and preservation/oxidation than Ba values alone (Grant et al., 2017). Down-core bulk magnetic property profiles of the studied sediments contain three main intervals: (1) representative sapropel intervals (i-156 and i-160; Figure 2, dark gray shaded bars), (2) weakly developed sapropel intervals (i-158, i-162, and i-166; Figure 2, light gray shaded bars), and (3) intervening marl intervals.

High Ba concentrations are observed in representative sapropels (e.g., i-156 and i-160), which indicates that sapropel deposition occurred under high productivity conditions (Figure 2a). Sapropels are also characterized by S and Fe enrichments (Figures 2c and 2d), which attests to diagenetic iron remobilization through iron sulfide formation, mostly pyrite, under sulfate-reducing conditions driven by the accumulation and microbial degradation of organic matter (Calvert & Fontugne, 2001; Pruyers et al., 1993; Thomson et al., 1995; van Santvoort et al., 1997; Warning & Brumsack, 2000; Wehausen & Brumsack, 2000). Ti/Al ratios reach minima within sapropels compared to the surrounding marls (Figure 2e), which indicate increased riverine input relative to eolian dust input during times of sapropel formation (Lourens et al., 2001). In weakly developed sapropels (e.g., i-158, i-162, and i-166), Ba contents increase compared to surrounding marls, but they have relatively lower values than in representative sapropels (Figure 2a). Less pronounced Ti/Al minima occur in weakly developed sapropels compared to representative sapropels (Figure 2e), which indicate less pronounced monsoon flooding from the Nile and wider North African margin. Slightly increased S and Fe concentrations are also observed in weakly developed sapropels (Figures 2b and 2c), which suggests that reducing conditions occurred, but were less strong, as would be expected for the

lower organic matter inputs. Ba and S contents are stable at near-zero values in marls, which represent background sedimentation in the eastern Mediterranean Sea between sapropels, while Fe concentration has a small peak in marls below i-162 (Figures 2a, 2c, and 2d). Across this thin interval, Ba values are enhanced slightly and Ti/Al has a small minimum, which suggest the presence of a so-called hidden sapropel that is not obvious visually because of postdepositional oxidation (Larrasoña et al., 2006). Ti/Al oscillates around high values of 0.07 in marls (Figure 2e), which reflects relatively lower fluvial discharge in these intervals.

## 4. Results

### 4.1. Magnetic Properties

Down-core profiles of magnetic parameters are shown in Figure 3. The magnetic parameters  $\chi$ , ARM, and SIRM are mainly sensitive to ferrimagnetic mineral concentration (Chaparro et al., 2008; Lascu, 2010; H. Liu et al., 2003). These parameters drop rapidly to low values in the upper parts of sapropels and remain low throughout underlying dissolution intervals. For representative sapropels,  $\chi$ , ARM, and SIRM recover rapidly in oxidation fronts, where they typically reach their highest values (Figures 3b–3d). These parameters have intermediate values in the marls that occur between sapropels.  $\chi$ , ARM, and SIRM have approximately similar variations with depth, except that peak values in oxidation fronts are more pronounced for ARM and SIRM.  $\chi$ , ARM, and SIRM values follow similar trends for weakly developed sapropel i-158 as for representative sapropels, except that it has a less developed oxidation front. These parameters decrease slightly from the oxidation front in weakly developed sapropel i-166 to reach minima in the upper part of the sapropel and then increase from the middle of the sapropel (Figures 3b–3d). For marls below representative sapropels,  $\chi$ , ARM, and SIRM recover gradually from the dissolution intervals and reach high values at the next underlying oxidation front. For marls underlying weakly developed sapropels,  $\chi$ , ARM, and SIRM recover rapidly from the lower part of the sapropels (Figures 3b–3d).

$IRM_{@AF120\text{ mT}}$  values represent magnetic minerals with coercivity larger than 120 mT, which is mainly high-coercivity hematite. Such hematite-dominated parameters have been used previously as eolian dust proxies in marine sediments (Larrasoña, Roberts, Rohling, et al., 2003). Compared to weakly developed sapropels and marls,  $IRM_{@AF120\text{ mT}}$  has clearly lower values in representative sapropels that decrease significantly from oxidation fronts to the lower parts of sapropels and then increase gradually within dissolution intervals (Figure 3e). This is indicative of a greater resistance of hematite to reductive dissolution compared to magnetite (e.g., Poulton et al., 2004; Roberts, 2015; Snowball, 1993) and indicates that the  $IRM_{@AF120\text{ mT}}$  proxy can provide a valuable indicator of subtle variations in hematite input (Larrasoña, Roberts, Stoner, et al., 2003). High  $IRM_{@AF120\text{ mT}}$  values occur in the lower parts of weakly developed sapropels, while low values occur in the upper or middle parts of these sapropels.

Magnetic grain-size sensitive parameters ( $\chi_{ARM}/\chi$ , ARM/SIRM, and SIRM/ $\chi$ ) (J. King et al., 1982; J. W. King & Channell, 1991) have roughly parallel variations (Figures 3f–3h). Oxidized sediments at the tops of sapropels are marked by larger proportions of fine SD/vortex state grains, as indicated by the highest  $\chi_{ARM}/\chi$ , ARM/SIRM, and SIRM/ $\chi$  values that drop rapidly to minima in the middle of sapropel layers and throughout the dissolution intervals (Figures 3f–3h). High values of these ratios also occur in the oxidation fronts of weakly developed sapropel i-166 and in the middle of i-158. Low values occur in the lower parts of weakly developed sapropels and underlying marls, which indicates the dominance of coarser magnetic minerals (Figures 3f–3h). In the lower parts of the marl intervals, grain-size sensitive parameters increase markedly toward the underlying oxidation fronts.

The S-ratio indicates the relative contribution of low- to high-coercivity magnetic minerals. S-ratio values are distinctly low in dissolution intervals and in underlying marls, while the rest of the studied sequence have relatively stable values around 0.97 (Figure 3i). This indicates an increased relative importance of high-coercivity minerals (hematite) within dissolution intervals.

### 4.2. Magnetic Mineralogy

All measured ZFC and FC curves contain distinctive inflections associated with the Verwey transition temperature for magnetite ( $T_v$ ) at ~95 K, except for a sample from the dissolution interval of representative sapropel i-160 (Figure 4c). Samples from the oxidation fronts of representative sapropel i-160 and weakly developed sapropel i-166 have two inflections at ~95 and ~110 K in SIRM derivative curves (Figures 4b

and 4e). This double  $T_v$  feature represents the presence of both biogenic and inorganic magnetites (Chang et al., 2016). The double peak feature is less clear for a sample from the middle of weakly developed sapropel i-166 (Figure 4f), but it is obvious in weakly developed sapropel i-162 (Figure 4d). Remanence loss at  $\sim 95$  K is more pronounced compared to that at  $\sim 110$  K for samples from oxidation fronts (Figures 4b and 4e), and it is less pronounced for samples from the middle part of weakly developed sapropel i-162 (Figure 4d). The inflection at  $\sim 95$  K is due to biogenic magnetite (Chang et al., 2016).

TEM imaging of magnetic mineral extracts confirms the common presence of detrital titanomagnetite and biogenic magnetite particles within the studied sediments (Figures 4g–4o). Samples from oxidation fronts and weakly developed sapropels reveal the presence of abundant fine-grained biogenic magnetite particles (Figures 4g, 4h, 4j, 4l, and 4n). These crystals have well-defined morphologies (cubo octahedral, prismatic, and bullet shaped) and sizes within the SD size range for magnetite (Muxworthy & Williams, 2009) that are typical of magnetofossils (e.g., Bazylinski & Frankel, 2004; Chang et al., 2014; Kopp & Kirschvink, 2008; Petersen et al., 1986; Roberts et al., 2012). Clustering of biogenic magnetite particles in the TEM images is likely due to magnetofossil chain collapse during ultrasonication (e.g., Li et al., 2012) associated with sample preparation for magnetic extraction. Biogenic magnetite crystals are more abundant in oxidation fronts compared to sapropel layers. Titanomagnetite particles with sizes ranging from hundreds of nanometers (nm) to several micrometers ( $\mu\text{m}$ ) are observed in samples from dissolution intervals (Figure 4i) and weakly developed sapropels (Figures 4k, 4m, and 4o). When compared with LT results, samples with more abundant biogenic magnetite have a pronounced  $T_v$  signal at  $\sim 95$  K (Figures 4b, 4e, and 4f) while samples with less biogenic magnetite or only titanomagnetite have a pronounced  $T_v$  signal at  $\sim 110$  K or no clear  $T_v$  signal (Figures 4c and 4d), as discussed below.

### 4.3. FORC-PCA Unmixing

FORC-PCA unmixing results for all samples are shown in Figure 5. Three distinctive clusters occur on the principal component 1 (PC1)-PC2 plane (Figure 5a). Group 1 (G1) and Group 2 (G2) represent samples from the dissolution intervals of sapropels i-160 and i-156, respectively. PC scores in Group 3 (G3) are more tightly aggregated and represent the rest of the samples. As illustrated in Figures 5b–5d, G1 has elongated FORC distributions along the  $B_c$  axis, which indicates the presence of noninteracting SD particles. G2 and G3 have mixed features with SD particles with peak coercivity of 10–20 mT and vertical spreading along the  $B_u$  axis (Figures 5c and 5d), which is indicative of vortex state particles (Roberts et al., 2017; Lascu et al., 2018). Compared to G3 (Figure 5d), G2 has a lower peak coercivity for SD particles (Figure 5c).

As is clear in Figure 5a, there is considerable variability within G3, so we extend FORC-PCA further here to assess these variations within 28 samples from oxidation fronts, the middles of sapropels, and marls. Two EMs are identified within this group (Figure 6a). EM1 is represented by vortex state particles (Figure 6b), while EM2 is dominated by a central ridge feature, which is characteristic of biogenic magnetite (Figure 6c; e.g., Egli et al., 2010; Roberts et al., 2012). Down-core variations of the magnetization contributions of the two EMs were calculated from FORC-PCA unmixing results and are shown in Figure 6d. EM1, which represents coarser detrital magnetic minerals, is enhanced in marls and is much less abundant in oxidation fronts (Figure 6d, blue). EM2, which represents biogenic magnetite, is enhanced in oxidation fronts, especially for representative sapropels, and makes a much lower contribution in other intervals (Figure 6d, red).

## 5. Discussion

### 5.1. Detection of Biogenic Magnetic Minerals

It has been suggested that magnetofossils produced by MTB formed in the oxidized zone at the tops of sapropels (Kruiver & Passier, 2001; Passier et al., 2001; Passier & Dekkers, 2002). Passier et al. (2001) reported that the high ARM and coercivity of magnetite, fine particle size, and low dispersion of the fitted IRM component in the vicinity of oxidation fronts is most likely associated with magnetofossils. Kruiver and Passier (2001) analyzed coercivities in the most recent sapropel, which indicated strongly that biogenic magnetite formed in the active oxidation front. LT results of Passier and Dekkers (2002) indicated that superparamagnetic (SP) particles also exist in oxidized zones above sapropels. Although these studies provide strong indications of the presence of biogenic magnetite in oxidation fronts, it has not been proven by direct TEM imaging of magnetofossils.

Our FORC analyses provide a direct indication that central ridge features are observed not only in oxidation fronts but also in weakly developed sapropels and marls. FORC-PCA unmixing results indicate that magnetofossils appear to occur throughout the studied sequence except within intervals with strong magnetic mineral dissolution (Figure 6d). TEM observations and LT measurements confirm that EM2 identified in FORC-PCA analysis is dominated by magnetofossils and that biogenic magnetite particles occur in most of the studied sediments (Figures 4b, 4d–4h, 4j, 4l, and 4n). Membrane-bound, SD magnetite crystals are synthesized intracellularly by MTB in a genetically controlled process. MTB live within strictly limited environments, where temperature, pH, external Fe concentration, external magnetic fields, static or dynamic fluid conditions, oxygen concentration, and nutrient availability or concentrations can all affect magnetosome biomineralization in MTB (Yan et al., 2012). Widespread magnetofossils in the studied sediments indicate that sustained conditions with nitrogenous to ferruginous diagenesis existed, which favor continued MTB activity and preservation (Roberts et al., 2011; Larrasoña et al., 2012). In contrast, burial into sulfidic diagenetic zones, such as during periods of sapropel formation, will cause extensive magnetite dissolution, particularly of fine-grained magnetofossils (e.g., Roberts, 2015). We do not observe evidence for magnetosomal greigite (e.g., Reinholdsson et al., 2013), which is most likely to be preserved if greigite-producing MTB were active during periods of sapropel formation. The distinctive magnetic properties associated with magnetosomal greigite (e.g., Reinholdsson et al., 2013) have only been observed for Type 1 sapropels, which were not studied here; if such greigite was initially present, it is unlikely to have survived drying and oxidation of the core after recovery (e.g., Roberts et al., 1999).

### 5.2. Biogenic Magnetic Mineral Abundances

The stratigraphic distribution of EM2 identified from FORC-PCA unmixing demonstrates that biogenic magnetite concentrations are high at oxidation fronts (Figures 6d and 7f), which indicates that redox conditions at oxidation fronts provide a habitat that enables growth of MTB populations. On the one hand, MTB productivity requires sufficient organic carbon to release bioavailable iron. On the other hand, the organic carbon flux cannot be too high because a sulfidic diagenetic environment would form in which magnetite dissolves to prevent magnetofossil preservation (Chang et al., 2018; Larrasoña et al., 2014; Roberts et al., 2011). Magnetofossil preservation in sediments tends to reflect competition between MTB productivity and preservation (e.g., Dinarès-Turell et al., 2003; Hesse, 1994; Kopp et al., 2009), which can be an indicator of sediment oxygenation levels (e.g., Chang et al., 2018; Hesse, 1994; Kopp et al., 2007, 2009; Kopp & Kirschvink, 2008; Lippert & Zachos, 2007; Yamazaki, 2012; Yamazaki & Ikehara, 2012).  $\text{Fe}^{2+}$  is mobilized upward by pyrite oxidation at the tops of sapropels when bottom waters were reoxygenated immediately after periods of sapropel formation (Passier et al., 2001; van Santvoort et al., 1996) and is precipitated as mixed valence iron oxides (Figure 8). MTB abundances decrease when moving upward from the top of oxidation fronts due to the gradually reduced concentration of liberated  $\text{Fe}^{2+}$  (e.g., i-160). Coincidence between ARM values and EM2 abundance variations in the oxidation fronts of sapropels i-156 and i-160 (Figures 7e and 7f) indicates that the biogenic magnetite concentration is responsible for the enhanced magnetization of oxidation fronts. In magnetic mineral dissolution intervals, such as within and below representative sapropels, reductive dissolution has removed fine ferrimagnetic particles, so that magnetofossils are preserved rarely. Strong correlation between EM2 and ARM indicates that normal sedimentary conditions represented by marls were also suitable for MTB, although magnetizations are lower. This magnetofossil abundance variation probably reflects variations in nutrients and redox gradient strength in which MTB lived. Observed biogenic magnetite variations around oxidation fronts are consistent with the rationale of Hesse (1994) that variable oxygenation leads to variable overall MTB production and preservation.

### 5.3. Detection of Detrital Magnetic Minerals

It has been argued that eolian dust is a major sediment source for the eastern Mediterranean Sea (Kruiver & Passier, 2001; Larrasoña, Roberts, Rohling, et al., 2003; Lourens et al., 2001).  $\text{IRM}_{@AF120 \text{ mT}}$  has been used as an eolian dust proxy in this region (Larrasoña, Roberts, Rohling, et al., 2003). SIRM has strong similarities with  $\text{IRM}_{@AF120 \text{ mT}}$  except in representative sapropels and dissolution intervals, where magnetite dissolution has occurred (Figures 7a and 7b). The value of  $\text{IRM}_{@AF120 \text{ mT}}$  as a high-coercivity eolian hematite proxy has been proven in several studies (Larrasoña et al., 2015; Larrasoña, Roberts, Rohling, et al., 2003; Larrasoña, Roberts, Stoner, et al., 2003), so that the strong similarity between SIRM and  $\text{IRM}_{@AF120 \text{ mT}}$

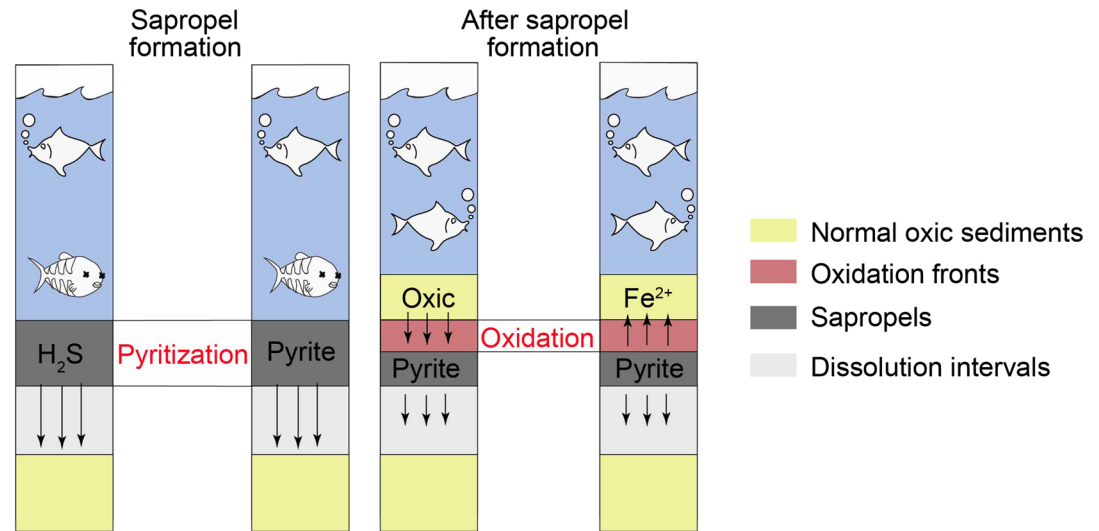


**Figure 8.** Illustration of the effects of variable bottom water ventilation and  $\text{Fe}^{2+}$  mobilization on nonsteady-state diagenesis in eastern Mediterranean sediments (characteristic of a Type 2 sapropel; Larrasoña, Roberts, Stoner, et al., 2003). During times of sapropel formation, bottom waters were sulfidic so that  $\text{H}_2\text{S}$  diffused downward into sediments below sapropels to cause magnetite dissolution, pyrite formation, and magnetization loss. When bottom waters are reventilated, oxygen diffuses downward into formerly sulfidic sediments, which produces an oxidation front where  $\text{Fe}^{2+}$  is mobilized upward by pyrite oxidation (Passier et al., 2001; Passier and Dekkers, 2002). Figure produced by Dr. Juan-Cruz Larrasoña and used by Roberts (2015).

suggests that the magnetic minerals represented by SIRM must also have a dominantly eolian source outside of sapropel dissolution intervals. This interpretation is supported by the observation that there are no large magnetic mineral influxes in the more humid periods associated with representative and weakly developed sapropels, which would be taken to indicate a significant fluvial input of detrital magnetic minerals. Moreover, SIRM and  $\text{IRM}_{@AF120\text{ mT}}$  have two distinct linear relationships in marls and within dissolution intervals (Figure 9). The linearity indicates that magnetic minerals within marls have a similar coercivity distribution, which is more likely to represent a single source rather than material from multiple sources.

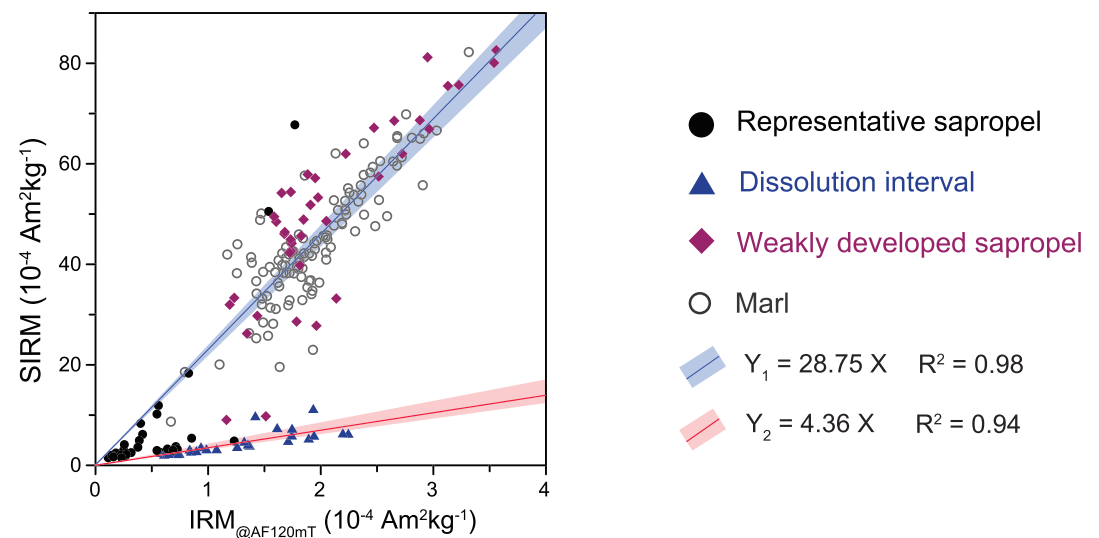


**Figure 9.** Relationship between SIRM and the  $\text{IRM}_{@AF120\text{ mT}}$  dust proxy. Data are shown for representative sapropels (black circles) and their dissolution fronts (blue triangles), weakly developed sapropels (magenta diamonds), and intercalated marls (gray circles).

Kruiver and Passier (2001) also observed that their interpreted magnetite and hematite components have constant ratios for Holocene sediments, which indicates that the magnetic minerals have the same source.

LT measurements and TEM observations, coupled with FORC unmixing results, further indicate that detrital magnetite is the magnetically dominant magnetic mineral in the studied sediments. LT measurements indicate that detrital magnetite particles are dominant in weakly developed sapropels (Figures 4d and 4f). TEM observations confirm that coarse titanomagnetite is preserved in almost all samples (Figures 6i, 6k, 6m, and 6o; note that not all titanomagnetite TEM images are shown). FORC unmixing results for G1 and G2 (Figure 5) from the two studied representative sapropels not only demonstrate the occurrence of detrital magnetite in representative sapropels and underlying dissolution intervals but also that different grain sizes occur in different intervals. A representative FORC diagram for G1 has an SP/SD feature with no vortex or MD signal (Figure 5b), which indicates that the magnetic minerals were reduced to a smaller size during dissolution (e.g., Roberts et al., 2018). In contrast, a representative FORC diagram for G2 has a coarser vortex state feature (Figure 5c), which indicates that less magnetite dissolution has occurred in sapropel i-156 compared to i-160. The presence of dissolution intervals indicates that organic matter accumulation was sufficient to produce excess sulfide (Figure 8), which migrated downward to cause magnetite dissolution (e.g., Larrasoana et al., 2006; Larrasoana, Roberts, Stoner, et al., 2003; Passier et al., 1996, 1999; Roberts, 2015), where dissolution intensity decreases gradually with increasing depth below sapropels. Samples from G2 lie further below their overlying sapropel than samples from G1 (Figure 5e), which could explain their coarser grain sizes. Additionally, FORC diagrams (Figures 5d and 6b) for marl and weakly developed sapropel samples have dominantly vortex state behavior (cf. Lascau et al., 2018; Roberts et al., 2017) that reveals the dominance of coarse magnetite, with no clear evidence for SP particles (Kruiver & Passier, 2001). The absolute contribution of biogenic magnetite is generally small outside of oxidation fronts (Figures 6d and 7f), and EM1 mainly reflects nonbiogenic magnetic mineral concentrations outside of oxidation fronts. Similar trends among EM1, SIRM, and  $IRM_{@AF120\text{ mT}}$  indicate that eolian detrital magnetite is the main magnetic mineral in the studied sequence except for within oxidation fronts and dissolution intervals (Figures 7a–7d).

#### 5.4. Benefits and Limitations of Advanced Methods

Advanced environmental magnetic methods, such as FORC-PCA and LT measurements, with supplementary TEM observations, can provide direct indications of mineral magnetic assemblages and can enable estimation of end member abundances. However, these techniques are time consuming, so they tend not to be used to develop high-resolution records. Conventional bulk magnetic parameters provide a rapid and non-destructive means of assessing continuous environmental magnetic variations. Those parameters mainly enable detection of magnetite or other ferrimagnetic minerals. If the aims of a study are to detect continuous ferrimagnetic variations, conventional bulk measurements are sufficient. Otherwise, the combined use of conventional bulk magnetic parameters and advanced techniques provides improved diagnosis of processes responsible for environmental magnetic signals.

## 6. Conclusions

We have applied both conventional bulk and more time-consuming advanced techniques to identify magnetic minerals within complexly mixed magnetic mineral assemblages in eastern Mediterranean sediments. Conventional bulk magnetic parameters provide continuous records of important environmental variations that have contrasting magnetic signatures, such as oxidation fronts and dissolution intervals (Figure 8). However, these parameters do not necessarily enable identification of multiple magnetic mineral components preserved in the studied sediments. Advanced environmental magnetic methods, such as LT and FORC measurements, provide crucial direct indications of mineral magnetic assemblages that enable calculation of the abundances of different end members.

FORC and LT results, along with TEM images, provide a clear demonstration that biogenic magnetite formed at oxidation fronts above eastern Mediterranean sapropels (Figure 8). The abundance of biogenic magnetite (quantified through FORC-PCA) indicates that markedly enhanced biogenic magnetite abundances occur at oxidation fronts. This indicates that the strong redox gradient produced when sulfidic sapropelic sediments are exposed to oxygenated bottom waters (Figure 8) provides a suitable habitat for magnetotactic bacteria. Our results also indicate that biogenic magnetite is present throughout the studied sediments, with the exception of sulfidic diagenetic intervals, in which magnetite dissolves. Furthermore,

we find that detrital magnetite dominates the sediment magnetization except at oxidation fronts. Overall, our results emphasize the value of conventional continuous bulk magnetization records for environmental magnetic analysis, where the use of advanced diagnostic methods adds significant interpretive power to understand the processes responsible for environmental signals.

## Data Availability Statement

The data presented in this paper can be found in the RMAG portal (rock magic database) of the Magnetics Information Consortium (<http://earthref.org/MAGIC/>).

## Acknowledgments

This work was supported financially by the Australian Research Council (grants DP160100805 and DE190100042) and the National Natural Science Foundation of China (grants 41920104009 and 41890843). Yao Qian is supported by the China Scholarship Council for her study at ANU. TEM experiments were performed at the Electron Microscope Laboratory, IGG-CAS (Beijing, China), with the kind assistance of TEM engineers Mrs. Lixin Gu and Tang Xu.

## References

- Banerjee, S. K., King, J., & Marvin, J. (1981). A rapid method for magnetic granulometry with applications to environmental studies. *Geophysical Research Letters*, *8*(4), 333–336. <https://doi.org/10.1029/GL008i004p00333>
- Bazylinski, D. A., & Frankel, R. B. (2004). Magnetosome formation in prokaryotes. *Nature Reviews Microbiology*, *2*(3), 217–230. <https://doi.org/10.1038/nrmicro842>
- Bloemendal, J., King, J. W., Hall, F. R., & Doh, S. J. (1992). Rock magnetism of Late Neogene and Pleistocene deep-sea sediments—Relationship to sediment source, diagenetic processes, and sediment lithology. *Journal of Geophysical Research*, *97*(B4), 4361–4375. <https://doi.org/10.1029/91JB03068>
- Calvert, S. E., & Fontugne, M. R. (2001). On the late Pleistocene-Holocene sapropel record of climatic and oceanographic variability in the eastern Mediterranean. *Paleoceanography*, *16*(1), 78–94. <https://doi.org/10.1029/1999PA000488>
- Chang, L., Harrison, R. J., Zeng, F., Berndt, T. A., Roberts, A. P., Heslop, D., & Zhao, X. (2018). Coupled microbial bloom and oxygenation decline recorded by magnetofossils during the Palaeocene-Eocene Thermal Maximum. *Nature Communications*, *9*(1), 1–9. <https://doi.org/10.1038/s41467-018-06472-y>
- Chang, L., Heslop, D., Roberts, A. P., Rey, D., & Mohamed, K. J. (2016). Discrimination of biogenic and detrital magnetite through a double Verwey transition temperature. *Journal of Geophysical Research: Solid Earth*, *121*, 3–14. <https://doi.org/10.1002/2015JB012485>
- Chang, L., Roberts, A. P., Winklhofer, M., Heslop, D., Dekkers, M. J., Krijgsman, W., et al. (2014). Magnetic detection and characterization of biogenic magnetic minerals: A comparison of ferromagnetic resonance and first-order reversal curve diagrams. *Journal of Geophysical Research: Solid Earth*, *119*, 6136–6158. <https://doi.org/10.1002/2014JB011213>
- Channell, J. E. T., Harrison, R. J., Lascu, I., McCave, I. N., Hibbert, F. D., & Austin, W. E. (2016). Magnetic record of deglaciation using FORC-PCA, sortable-silt grain size, and magnetic excursion at 26 ka, from the Rockall Trough (NE Atlantic). *Geochemistry, Geophysics, Geosystems*, *17*, 1823–1841. <https://doi.org/10.1002/2016GC006300>
- Channell, J. E. T., & Hawthorne, T. (1990). Progressive dissolution of titanomagnetites at ODP Site 653 (Tyrrhenian Sea). *Earth and Planetary Science Letters*, *96*(3–4), 469–480. [https://doi.org/10.1016/0012-821x\(90\)90021-0](https://doi.org/10.1016/0012-821x(90)90021-0)
- Chaparro, M. A. E., Sinito, A. M., Ramasamy, V., Marinelli, C., Chaparro, M. A. E., Mullainathan, S., & Murugesan, S. (2008). Magnetic measurements and pollutants of sediments from Cauvery and Palaru River, India. *Environmental Geology*, *56*(2), 425–437. <https://doi.org/10.1007/s00254-007-1180-1>
- de Lange, G. J., Thomson, J., Reitz, A., Slomp, C. P., Speranza Principato, M., Erba, E., & Corselli, C. (2008). Synchronous basin-wide formation and redox-controlled preservation of a Mediterranean sapropel. *Nature Geoscience*, *1*, 606–610. <https://doi.org/10.1038/ngeo283>
- Dekkers, M. J., Langereis, C. G., Vriend, S. P., van Santvoort, P. J. M., & de Lange, G. J. (1994). Fuzzy c-means cluster analysis of early diagenetic effects on natural remanent magnetisation acquisition in a 1.1 Myr piston core from the Central Mediterranean. *Physics of the Earth and Planetary Interiors*, *85*(1–2), 155–171. [https://doi.org/10.1016/0031-9201\(94\)90014-0](https://doi.org/10.1016/0031-9201(94)90014-0)
- Dinarès-Turell, J., Hoogakker, B. A. A., Roberts, A. P., Rohling, E. J., & Sagnotti, L. (2003). Quaternary climatic control of biogenic magnetite production and eolian dust input in cores from the Mediterranean Sea. *Palaeogeography, Palaeoclimatology, Palaeoecology*, *190*, 195–209. [https://doi.org/10.1016/s0031-0182\(02\)00605-3](https://doi.org/10.1016/s0031-0182(02)00605-3)
- Egli, R. (2013). VARIFORC: An optimized protocol for calculating non-regular first-order reversal curve (FORC) diagrams. *Global and Planetary Change*, *110*, 302–320. <https://doi.org/10.1016/j.gloplacha.2013.08.003>
- Egli, R., Chen, A. P., Winklhofer, M., Kodama, K. P., & Horng, C. S. (2010). Detection of noninteracting single domain particles using first-order reversal curve diagrams. *Geochemistry, Geophysics, Geosystems*, *11*, Q01Z11. <https://doi.org/10.1029/2009GC002916>
- Emeis, K. C., Robertson, A. H. F., & Richter, C. (1996). Shipboard Scientific Party ODP Leg 160. Ocean Drilling Program, College Station, TX, (972 pp.).
- Emeis, K. C., Sakamoto, T., Wehausen, R., & Brumsack, H. J. (2000). The sapropel record of the eastern Mediterranean Sea—Results of Ocean Drilling Program Leg 160. *Palaeogeography, Palaeoclimatology, Palaeoecology*, *158*(3–4), 371–395. [https://doi.org/10.1016/S0031-0182\(00\)00059-6](https://doi.org/10.1016/S0031-0182(00)00059-6)
- Evans, M. E., & Heller, F. (2003). *Environmental magnetism: Principles and applications of enviro magnetics* (p. 299). San Diego: Academic Press.
- Grant, K. M., Grimm, R., Mikolajewicz, U., Marino, G., Ziegler, M., & Rohling, E. J. (2016). The timing of Mediterranean sapropel deposition relative to insolation, sea-level and African monsoon changes. *Quaternary Science Reviews*, *140*, 125–141. <https://doi.org/10.1016/j.quascirev.2016.03.026>
- Grant, K. M., Rohling, E. J., Westerhold, T., Zabel, M., Heslop, D., Konijnendijk, T., & Lourens, L. (2017). A 3 million year index for North African humidity/aridity and the implication of potential pan-African humid periods. *Quaternary Science Reviews*, *171*, 100–118. <https://doi.org/10.1016/j.quascirev.2017.07.005>
- Harrison, R. J., & Feinberg, J. M. (2008). FORCinel: An improved algorithm for calculating first-order reversal curve distributions using locally weighted regression smoothing. *Geochemistry, Geophysics, Geosystems*, *9*, Q05016. <https://doi.org/10.1029/2008GC001987>
- Harrison, R. J., Muraszko, J., Heslop, D., Lascu, I., Muxworthy, A. R., & Roberts, A. P. (2018). An improved algorithm for unmixing first-order reversal curve diagrams using principal component analysis. *Geochemistry, Geophysics, Geosystems*, *19*, 1595–1610. <https://doi.org/10.1029/2018GC007511>

- Heslop, D. (2015). Numerical strategies for magnetic mineral unmixing. *Earth-Science Reviews*, *150*, 256–284. <https://doi.org/10.1016/j.earscirev.2015.07.007>
- Heslop, D., von Dobeneck, T., & Höcker, M. (2007). Using non-negative matrix factorization in the “unmixing” of diffuse reflectance spectra. *Marine Geology*, *241*(1–4), 63–78. <https://doi.org/10.1016/j.margeo.2007.03.004>
- Hesse, P. P. (1994). Evidence for bacterial palaeoecological origin of mineral magnetic cycles in oxic and sub-oxic Tasman Sea sediments. *Marine Geology*, *117*(1–4), 1–17. [https://doi.org/10.1016/0025-3227\(94\)90003-5](https://doi.org/10.1016/0025-3227(94)90003-5)
- Higgs, N. C., Thomson, J., Wilson, T. R. S., & Croudace, I. W. (1994). Modification and complete removal of eastern Mediterranean sapropels by postdepositional oxidation. *Geology*, *22*, 423–426. [https://doi.org/10.1130/0091-7613\(1994\)022<0423:MACROE>2.3.CO;2](https://doi.org/10.1130/0091-7613(1994)022<0423:MACROE>2.3.CO;2)
- Hilgen, F. J. (1991). Astronomical calibration of Gauss to Matuyama sapropels in the Mediterranean and implication for the geomagnetic polarity time scale. *Earth and Planetary Science Letters*, *104*(2–4), 226–244. [https://doi.org/10.1016/0012-821x\(91\)90206-W](https://doi.org/10.1016/0012-821x(91)90206-W)
- Kent, D. V. (1982). Apparent correlation of palaeomagnetic intensity and climatic records in deep-sea sediments. *Nature*, *299*(5883), 538–539. <https://doi.org/10.1038/299538a0>
- King, J., Banerjee, S. K., Marvin, J., & Özdemir, Ö. (1982). A comparison of different magnetic methods for determining the relative grain-size of magnetite in natural materials: Some results from lake-sediments. *Earth and Planetary Science Letters*, *59*(2), 404–419. [https://doi.org/10.1016/0012-821x\(82\)90142-X](https://doi.org/10.1016/0012-821x(82)90142-X)
- King, J. W., & Channell, J. E. T. (1991). Sedimentary magnetism, environmental magnetism, and magnetostratigraphy. *Reviews of Geophysics*, *29*, 358–370. <https://doi.org/10.1002/rog.1991.29.s1.358>
- Kopp, R. E., & Kirschvink, J. L. (2008). The identification and biogeochemical interpretation of fossil magnetotactic bacteria. *Earth-Science Reviews*, *86*(1–4), 42–61. <https://doi.org/10.1016/j.earscirev.2007.08.001>
- Kopp, R. E., Raub, T. D., Schumann, D., Vali, H., Smirnov, A. V., & Kirschvink, J. L. (2007). Magnetofossil spike during the Paleocene-Eocene thermal maximum: Ferromagnetic resonance, rock magnetic, and electron microscopy evidence from Ancora, New Jersey, United States. *Paleoceanography*, *22*, PA4103. <https://doi.org/10.1029/2007PA001473>
- Kopp, R. E., Schumann, D., Raub, T. D., Powars, D. S., Godfrey, L. V., Swanson-Hysell, N. L., et al. (2009). An Appalachian Amazon? Magnetofossil evidence for the development of a tropical river-like system in the mid-Atlantic United States during the Paleocene-Eocene thermal maximum. *Paleoceanography*, *24*, PA4211. <https://doi.org/10.1029/2009PA001783>
- Kruiver, P. P., & Passier, H. F. (2001). Coercivity analysis of magnetic phases in sapropel S1 related to variations in redox conditions, including an investigation of the S ratio. *Geochemistry, Geophysics, Geosystems*, *2*(12). <https://doi.org/10.1029/2001GC000181>
- Larrasoaña, J. C., Liu, Q., Hu, P., Roberts, A. P., Mata, P., Civis, J., et al. (2014). Paleomagnetic and paleoenvironmental implications of magnetofossil occurrences in late Miocene marine sediments from the Guadalquivir Basin, SW Spain. *Frontiers in Microbiology*, *5*, 71. <https://doi.org/10.3389/fmicb.2014.00071>
- Larrasoaña, J. C., Roberts, A. P., Chang, L., Schellenberg, S. A., Fitz Gerald, J. D., Norris, R. D., & Zachos, J. C. (2012). Magnetotactic bacterial response to Antarctic dust supply during the Paleocene-Eocene thermal maximum. *Earth and Planetary Science Letters*, *333*, 122–133. <https://doi.org/10.1016/j.epsl.2012.04.003>
- Larrasoaña, J. C., Roberts, A. P., Hayes, A., Wehausen, R., & Rohling, E. J. (2006). Detecting missing beats in the Mediterranean climate rhythm from magnetic identification of oxidized sapropels (Ocean Drilling Program Leg 160). *Physics of the Earth and Planetary Interiors*, *156*(3–4), 283–293. <https://doi.org/10.1016/j.pepi.2005.04.017>
- Larrasoaña, J. C., Roberts, A. P., Liu, Q. S., Lyons, R., Oldfield, F., Rohling, E. J., & Heslop, D. (2015). Source-to-sink magnetic properties of NE Saharan dust in Eastern Mediterranean marine sediments: Review and paleoenvironmental implications. *Frontiers in Earth Science*, *3*, 19. <https://doi.org/10.3389/feart.2015.00019>
- Larrasoaña, J. C., Roberts, A. P., Rohling, E. J., Winklhofer, M., & Wehausen, R. (2003). Three million years of monsoon variability over the northern Sahara. *Climate Dynamics*, *21*(7–8), 689–698. <https://doi.org/10.1007/s00382-003-0355-z>
- Larrasoaña, J. C., Roberts, A. P., Stoner, J. S., Richter, C., & Wehausen, R. (2003). A new proxy for bottom-water ventilation in the eastern Mediterranean based on diagenetically controlled magnetic properties of sapropel-bearing sediments. *Paleogeography, Palaeoclimatology, Palaeoecology*, *190*, 221–242. [https://doi.org/10.1016/S0031-0182\(02\)00607-7](https://doi.org/10.1016/S0031-0182(02)00607-7)
- Lascu, I., Banerjee, S. K., & Berquó, T. S. (2010). Quantifying the concentration of ferrimagnetic particles in sediments using rock magnetic methods. *Geochemistry, Geophysics, Geosystems*, *11*, Q08Z19. <https://doi.org/10.1029/2010GC003182>
- Lascu, I., Einsle, J. F., Ball, M. R., & Harrison, R. J. (2018). The vortex state in geologic materials: A micromagnetic perspective. *Journal of Geophysical Research: Solid Earth*, *123*, 7285–7304. <https://doi.org/10.1029/2018JB015909>
- Lascu, I., Harrison, R. J., Li, Y., Muraszko, J. R., Channell, J. E. T., Piotrowski, A. M., & Hodell, D. A. (2015). Magnetic unmixing of first-order reversal curve diagrams using principal component analysis. *Geochemistry, Geophysics, Geosystems*, *16*, 2900–2915. <https://doi.org/10.1002/2015GC005909>
- Li, J. H., Wu, W. F., Liu, Q. S., & Pan, Y. X. (2012). Magnetic anisotropy, magnetostatic interactions and identification of magnetofossils. *Geochemistry, Geophysics, Geosystems*, *13*, Q10Z51. <https://doi.org/10.1029/2012GC004384>
- Lippert, P. C., & Zachos, J. C. (2007). A biogenic origin for anomalous fine-grained magnetic material at the Paleocene-Eocene boundary at Wilson Lake, New Jersey. *Paleoceanography*, *22*, PA4104. <https://doi.org/10.1029/2007PA001471>
- Liu, H., Zhu, R. X., & Li, G. X. (2003). Rock magnetic properties of the fine-grained sediment on the outer shelf of the East China Sea: Implication for provenance. *Marine Geology*, *193*(3–4), 195–206. [https://doi.org/10.1016/s0025-3227\(02\)00660-6](https://doi.org/10.1016/s0025-3227(02)00660-6)
- Liu, Q., Roberts, A. P., Larrasoaña, J. C., Banerjee, S. K., Guyodo, Y., Tauxe, L., & Oldfield, F. (2012). Environmental magnetism: Principles and applications. *Reviews of Geophysics*, *50*, RG4002. <https://doi.org/10.1029/2012RG000393>
- Liu, Q. S., Larrasoaña, J. C., Torrent, J., Roberts, A. P., Rohling, E. J., Liu, Z. F., & Jiang, Z. X. (2012). New constraints on climate forcing and variability in the circum-Mediterranean region from magnetic and geochemical observations of sapropels S1, S5 and S6. *Paleogeography, Palaeoclimatology, Palaeoecology*, *333*, 1–12. <https://doi.org/10.1016/j.palaeo.2012.02.036>
- Lourens, L. J., Antonarakou, A., Hilgen, F. J., van Hoof, A. A. M., Vergnaud-Grazzini, C., & Zachariasse, W. J. (1996). Evaluation of the Plio-Pleistocene astronomical timescale. *Paleoceanography*, *11*(4), 391–413. <https://doi.org/10.1029/96PA01125>
- Lourens, L. J., Wehausen, R., & Brumsack, H. J. (2001). Geological constraints on tidal dissipation and dynamical ellipticity of the Earth over the past three million years. *Nature*, *409*(6823), 1029–1033. <https://doi.org/10.1038/35059062>
- Maher, B. A., & Thompson, R. (Eds) (1999). *Quaternary Climates, Environments and Magnetism* (p. 390). Cambridge: Cambridge University Press.
- Muxworthy, A. R., & Williams, W. (2009). Critical superparamagnetic/single-domain grain sizes in interacting magnetite particles: Implications for magnetosome crystals. *Journal of the Royal Society Interface*, *6*(41), 1207–1212. <https://doi.org/10.1098/rsif.2008.0462>

- Nijenhuis, I. A., Bosch, H. J., Damste, J. S. S., Brumsack, H. J., & de Lange, G. J. (1999). Organic matter and trace element rich sapropels and black shales: A geochemical comparison. *Earth and Planetary Science Letters*, *169*(3–4), 277–290. [https://doi.org/10.1016/S0012-821x\(99\)00083-7](https://doi.org/10.1016/S0012-821x(99)00083-7)
- Oldfield, F., Darnley, I., Yates, G., France, D. E., & Hilton, J. (1992). Storage diagenesis versus sulphide authigenesis: Possible implications in environmental magnetism. *Journal of Palaeolimnology*, *7*, 179–189. <https://doi.org/10.1007/bf00181713>
- Passier, H. F., de Lange, G. J., & Dekkers, M. J. (2001). Magnetic properties and geochemistry of the active oxidation front and the youngest sapropel in the eastern Mediterranean Sea. *Geophysical Journal International*, *145*(3), 604–614. <https://doi.org/10.1046/j.0956-540x.2001.01394.x>
- Passier, H. F., & Dekkers, M. J. (2002). Iron oxide formation in the active oxidation front above sapropel S1 in the eastern Mediterranean Sea as derived from low-temperature magnetism. *Geophysical Journal International*, *150*(1), 230–240. <https://doi.org/10.1046/j.1365-246X.2002.01704.x>
- Passier, H. F., Middelburg, J. J., de Lange, G. J., & Böttcher, M. E. (1999). Modes of sapropel formation in the eastern Mediterranean: Some constraints based on pyrite properties. *Marine Geology*, *153*(1–4), 199–219. [https://doi.org/10.1016/S0025-3227\(98\)00081-4](https://doi.org/10.1016/S0025-3227(98)00081-4)
- Passier, H. F., Middelburg, J. J., van Os, B. J., & de Lange, G. J. (1996). Diagenetic pyritisation under eastern Mediterranean sapropels caused by downward sulphide diffusion. *Geochimica et Cosmochimica Acta*, *60*(5), 751–763. [https://doi.org/10.1016/0016-7037\(95\)00419-X](https://doi.org/10.1016/0016-7037(95)00419-X)
- Petersen, N., von Dobeneck, T., & Vali, H. (1986). Fossil bacterial magnetite in deep-sea sediments from the South-Atlantic Ocean. *Nature*, *320*(6063), 611–615. <https://doi.org/10.1038/320611a0>
- Pike, C. R., Roberts, A. P., & Verosub, K. L. (1999). Characterizing interactions in fine magnetic particle systems using first order reversal curves. *Journal of Applied Physics*, *85*(9), 6660–6667. <https://doi.org/10.1063/1.370176>
- Poulton, S. W., Krom, M. D., & Raiswell, R. (2004). A revised scheme for the reactivity of iron (oxyhydr) oxide minerals towards dissolved sulfide. *Geochimica et Cosmochimica Acta*, *68*(18), 3703–3715. <https://doi.org/10.1016/j.gca.2004.03.012>
- Pruyters, P. A., de Lange, G. J., Middelburg, J. J., & Hydes, D. J. (1993). The diagenetic formation of metal-rich layers in sapropel-containing sediments in the eastern Mediterranean. *Geochimica et Cosmochimica Acta*, *57*(3), 527–536. [https://doi.org/10.1016/0016-7037\(93\)90365-4](https://doi.org/10.1016/0016-7037(93)90365-4)
- Reinholdsson, M., Snowball, I., Zillén, L., Lenz, C., & Conley, D. J. (2013). Magnetic enhancement of Baltic Sea sapropels by greigite magnetofossils. *Earth and Planetary Science Letters*, *366*, 137–150. <https://doi.org/10.1016/j.epsl.2013.01.029>
- Richter, C., Hayashida, A., Guyodo, Y., Valet, J.-P., & Verosub, K. L. (1999). Magnetic intensity loss and core diagenesis in long-core samples from the East Cortez Basin and the San Nicolas Basin (California Borderland). *Earth, Planets and Space*, *51*, 329–336. <https://doi.org/10.1186/BF03352237>
- Roberts, A. P. (2015). Magnetic mineral diagenesis. *Earth-Science Reviews*, *151*, 1–47. <https://doi.org/10.1016/j.earscirev.2015.09.010>
- Roberts, A. P., Almeida, T. P., Church, N. S., Harrison, R. J., Heslop, D., Li, Y., et al. (2017). Resolving the origin of pseudo-single domain magnetic behavior. *Journal of Geophysical Research: Solid Earth*, *122*, 9534–9558. <https://doi.org/10.1002/2017JB014860>
- Roberts, A. P., Chang, L., Heslop, D., Florindo, F., & Larrasoana, J. C. (2012). Searching for single domain magnetite in the “pseudo-single-domain” sedimentary haystack: Implications of biogenic magnetite preservation for sediment magnetism and relative paleointensity determinations. *Journal of Geophysical Research*, *117*, B08104. <https://doi.org/10.1029/2012JB009412>
- Roberts, A. P., Florindo, F., Villa, G., Chang, L., Jovane, L., Bohaty, S. M., et al. (2011). Magnetotactic bacterial abundance in pelagic marine environments is limited by organic carbon flux and availability of dissolved iron. *Earth and Planetary Science Letters*, *310*(3–4), 441–452. <https://doi.org/10.1016/j.epsl.2011.08.011>
- Roberts, A. P., Pike, C. R., & Verosub, K. L. (2000). First-order reversal curve diagrams: A new tool for characterizing the magnetic properties of natural samples. *Journal of Geophysical Research*, *105*(B12), 28,461–28,475. <https://doi.org/10.1029/2000JB900326>
- Roberts, A. P., Stoner, J. S., & Richter, C. (1999). Diagenetic magnetic enhancement of sapropels from the eastern Mediterranean Sea. *Marine Geology*, *153*(1–4), 103–116. [https://doi.org/10.1016/S0025-3227\(98\)00087-5](https://doi.org/10.1016/S0025-3227(98)00087-5)
- Roberts, A. P., Zhao, X., Harrison, R. J., Heslop, D., Muxworthy, A. R., Rowan, C. J., et al. (2018). Signatures of reductive magnetic mineral diagenesis from unmixing of first-order reversal curves. *Journal of Geophysical Research: Solid Earth*, *123*, 4500–4522. <https://doi.org/10.1029/2018JB015706>
- Rohling, E. J. (1994). Review and new aspects concerning the formation of eastern Mediterranean sapropels. *Marine Geology*, *122*(1–2), 1–28. [https://doi.org/10.1016/0025-3227\(94\)90202-X](https://doi.org/10.1016/0025-3227(94)90202-X)
- Rohling, E. J., Marino, G., & Grant, K. M. (2015). Mediterranean climate and oceanography, and the periodic development of anoxic events (sapropels). *Earth-Science Reviews*, *143*, 62–97. <https://doi.org/10.1016/j.earscirev.2015.01.008>
- Rossignol-Strick, M. (1983). African monsoons, an immediate climate response to orbital insolation. *Nature*, *304*(5921), 46. <https://doi.org/10.1038/304046a0>
- Rossignol-Strick, M. (1985). Mediterranean Quaternary sapropels, an immediate response of the African monsoon to variation of insolation. *Palaeogeography, Palaeoclimatology, Palaeoecology*, *49*(3–4), 237–263. [https://doi.org/10.1016/0031-0182\(85\)90056-2](https://doi.org/10.1016/0031-0182(85)90056-2)
- Rossignol-Strick, M., Nesteroff, W., Olive, P., & Vergnaud-Grazzini, C. (1982). After the deluge: Mediterranean stagnation and sapropel formation. *Nature*, *295*(5845), 105. <https://doi.org/10.1038/295105a0>
- Sakamoto, T., Janecek, T., & Emeis, K.-C. (1998). Continuous sedimentary sequences from the eastern Mediterranean Sea: Composite depth sections. In A. H. F. Robertson, K.-C. Emeis, C. Richter, & A. Camerlenghi (Eds.), *Proceedings of the Ocean Drilling Program Scientific Results* (Vol. 160, pp. 37–59). College Station, TX: Ocean Drilling Program.
- Schenau, S. J., Antonarakou, A., Hilgen, F. J., Lourens, L. J., Nijenhuis, I. A., van der Weijden, C. H., & Zachariasse, W. J. (1999). Organic-rich layers in the Metochia section (Gavdos, Greece): Evidence for a single mechanism of sapropel formation during the past 10 My. *Marine Geology*, *153*(1–4), 117–135. [https://doi.org/10.1016/S0025-3227\(98\)00086-3](https://doi.org/10.1016/S0025-3227(98)00086-3)
- Schlitzer, R. (2014). Ocean Data View. <http://odv.awi.de>
- Snowball, I. F. (1993). Geochemical control of magnetite dissolution in subarctic lake sediments and the implications for environmental magnetism. *Journal of Quaternary Science*, *8*(4), 339–346. <https://doi.org/10.1002/jqs.3390080405>
- Stoner, J. S., Richter, C., & Roberts, A. P. (1998). High resolution study of magnetic properties of sapropel-bearing sediments from ODP sites 966, 967, and 969, eastern Mediterranean Sea. In *Proceedings of the Ocean Drilling Program, Scientific Results* (Vol. 160, pp. 75–82). College Station, TX: Ocean Drilling Program.
- Thompson, R., & Oldfield, F. (1986). *Environmental magnetism* (p. 227). Winchester, Mass, USA: Allen and Unwin.
- Thompson, R., Stober, J. C., Turner, G. M., Oldfield, F., Bloemendal, J., Dearing, J. A., & Rummery, T. A. (1980). Environmental applications of magnetic measurements. *Science*, *207*(4430), 481–486. <https://doi.org/10.1126/science.207.4430.481>

- Thomson, J., Higgs, N. C., Wilson, T. R. S., Croudace, I. W., de Lange, G. J., & van Santvoort, P. J. M. (1995). Redistribution and geochemical behavior of redox-sensitive elements around S1, the most recent eastern Mediterranean sapropel. *Geochimica et Cosmochimica Acta*, 59(17), 3487–3501. [https://doi.org/10.1016/0016-7037\(95\)00232-O](https://doi.org/10.1016/0016-7037(95)00232-O)
- Thomson, J., Mercone, D., de Lange, G. J., & van Santvoort, P. J. M. (1999). Review of recent advances in the interpretation of eastern Mediterranean sapropel S1 from geochemical evidence. *Marine Geology*, 153, 77–89. [https://doi.org/10.1016/S0025-3227\(98\)00089-9](https://doi.org/10.1016/S0025-3227(98)00089-9)
- van Santvoort, P. J. M., de Lange, G. J., Langereis, C. G., Dekkers, M. J., & Paterné, M. (1997). Geochemical and paleomagnetic evidence for the occurrence of “missing” sapropels in eastern Mediterranean sediments. *Paleoceanography*, 12(6), 773–786. <https://doi.org/10.1029/97PA01351>
- van Santvoort, P. J. M., de Lange, G. J., Thomson, J., Cussen, H., Wilson, T. R. S., Krom, M. D., & Strohle, K. (1996). Active post-depositional oxidation of the most recent sapropel (S1) in sediments of the eastern Mediterranean Sea. *Geochimica et Cosmochimica Acta*, 60(21), 4007–4024. [https://doi.org/10.1016/S0016-7037\(96\)00253-0](https://doi.org/10.1016/S0016-7037(96)00253-0)
- Verosub, K. L., & Roberts, A. P. (1995). Environmental magnetism: Past, present, and future. *Journal of Geophysical Research*, 100(B2), 2175–2192. <https://doi.org/10.1029/94JB02713>
- Warning, B., & Brumsack, H. J. (2000). Trace metal signatures of eastern Mediterranean sapropels. *Palaeogeography, Palaeoclimatology, Palaeoecology*, 158(3–4), 293–309. [https://doi.org/10.1016/S0031-0182\(00\)00055-9](https://doi.org/10.1016/S0031-0182(00)00055-9)
- Wehausen, R., & Brumsack, H. J. (2000). Chemical cycles in Pliocene sapropel-bearing and sapropel-barren eastern Mediterranean sediments. *Palaeogeography, Palaeoclimatology, Palaeoecology*, 158(3–4), 325–352. [https://doi.org/10.1016/S0031-0182\(00\)00057-2](https://doi.org/10.1016/S0031-0182(00)00057-2)
- Yamazaki, T. (2008). Magnetostatic interactions in deep-sea sediments inferred from first-order reversal curve diagrams: Implications for relative paleointensity normalization. *Geochemistry, Geophysics, Geosystems*, 9, Q02005. <https://doi.org/10.1029/2007GC001797>
- Yamazaki, T. (2012). Paleoposition of the Intertropical Convergence Zone in the eastern Pacific inferred from glacial-interglacial changes in terrigenous and biogenic magnetic mineral fractions. *Geology*, 40(2), 151–154. <https://doi.org/10.1130/g32646.1>
- Yamazaki, T., & Ikehara, M. (2012). Origin of magnetic mineral concentration variation in the Southern Ocean. *Paleoceanography*, 27, PA2206. <https://doi.org/10.1029/2011PA002271>
- Yan, L., Zhang, S., Chen, P., Liu, H., Yin, H., & Li, H. (2012). Magnetotactic bacteria, magnetosomes and their application. *Microbiological Research*, 167(9), 507–519. <https://doi.org/10.1016/j.micres.2012.04.002>
- Zhao, X., Heslop, D., & Roberts, A. P. (2015). A protocol for variable-resolution first-order reversal curve measurements. *Geochemistry, Geophysics, Geosystems*, 16, 1364–1377. <https://doi.org/10.1002/2014GC005680>